Am J Transl Res 2023;15(5):3092-3114
www.ajtr.org /ISSN:1943-8141/AJTR0148971

Original Article

Identification of ferroptosis-associated biomarkers in Stanford type A aortic dissection based on machine learning

Hao Pan[1], Wei Lu[2], Zhifei Liu[1*], Yu Wang[1*]

[1]Department of Anesthesiology, Shandong Provincial Hospital Affiliated to Shandong First Medical University, Jinan, Shandong, China; [2]Department of Oral and Maxillofacial Surgery, Shandong Provincial Hospital Affiliated to Shandong First Medical University, Jinan, Shandong, China. [*]Equal contributors and co-corresponding authors.

Received January 5, 2023; Accepted April 10, 2023; Epub May 15, 2023; Published May 30, 2023

Abstract: Background: Stanford type A aortic dissection (STAAD) is a serious cardiovascular disease with a high mortality rate. Ferroptosis is closely associated with various diseases, including cardiovascular disease. However, the role of ferroptosis in the progression of STAAD remains unclear. Methods: Gene expression profiles of GSE52093, GSE98770, and GSE153434 datasets were downloaded from the Gene Expression Omnibus (GEO) database. Weighted gene co-expression network analysis (WGCNA), least absolute shrinkage and selection operator (LASSO), and support vector machine-recursive feature elimination (SVM-RFE) were performed to determine the ferroptosis-associated characteristic genes in STAAD. Receiver operating characteristic (ROC) curve analysis was performed to evaluate the diagnostic efficacy. Furthermore, immune cell infiltrations were analyzed using the CIBERSORT algorithm. Drug sensitivity analysis was conducted based on the CellMiner database. Results: A total of 65 differentially expressed ferroptosis-associated genes were screened. DAZAP1 and GABARAPL2 were identified as valuable diagnostic biomarkers for STAAD. A nomogram with high accuracy and reliability was constructed as a diagnostic tool for STAAD. Furthermore, immune infiltration analysis suggested that monocytes were higher in the STAAD group compared with the control group. DAZAP1 was positively correlated with monocytes, whereas GABARAPL2 was negatively correlated with monocytes. Pan-cancer analysis showed that DAZAP1 and GABARAPL2 were closely associated with the prognosis of various cancers. In addition, some antitumor drugs might be useful for the treatment of STAAD. Conclusion: DAZAP1 and GABARAPL2 might serve as potential diagnostic biomarkers for STAAD. Meanwhile, DAZAP1 and GABARAPL2 might be related to cancer and STAAD in terms of ferroptosis, which provides insights into developing new therapeutic approaches for STAAD.

Keywords: Stanford type A aortic dissection, ferroptosis, immune infiltration, characteristic genes, pan-cancer analysis, drug sensitivity

Introduction

Aortic dissection (AD) is a life-threatening cardiovascular disease with an incidence of 3.5-7.2 per 100,000 people annually [1, 2]. AD is characterized by tears of the intimal and medial layers of the aortic wall, resulting in the formation of true and false lumens [3]. The most common type of AD is Stanford type A AD (STAAD), which accounts for almost 75% of all cases of AD and has a high mortality rate of 90%, if left untreated [4, 5]. Early diagnosis and treatment as well as close follow-up of AD patients are essential to improve their survival rate [6]. Currently, open surgical repair is the most effective treatment strategy for STAAD, but it requires a high level of technology and an experienced center [7]. Despite improvements in diagnostic methods, operative approaches, and perioperative care, these patients still have a high in-hospital mortality rate of 22% and an operative mortality rate of 18% [8, 9]. The main pathological mechanisms underlying AD include smooth muscle cell (SMC) alteration, extracellular matrix degradation, and inflammatory cell infiltration [10]. However, the potential molecular mechanisms underlying AD remain poorly understood. Therefore, exploring the pathogen-

esis of AD at the gene expression levels may provide new insights into diagnosis and therapy, thereby improving the clinical outcomes.

With the development of high-throughput sequencing and DNA microarray, studies based on bioinformatics analysis have revealed that immune-, necroptosis-, and N6-methyladenosine (m6A)-related characteristic genes and their potential molecular pathways are closely related to the progression of STAAD [7, 11, 12]. Ferroptosis is a non-apoptotic and iron-dependent programmed cell death process, which is characterized by the production of free radicals and excessive accumulation of lipid peroxides [13]. Emerging evidence suggests that ferroptosis might be involved in AD progression by promoting SMC dysfunction [14]. Chen et al. revealed that BRD4770 prevents aortic dilation and AD occurrence in a mouse model by inhibiting SMC ferroptosis and inflammatory response [15]. Li et al. found that ferroptosis was activated during AD progression and ferroptosis of SMCs was regulated via the METTL3-SLC7A11/FSP1 axis [16]. Moreover, liproxstatin-1 was found to attenuate aortic degeneration and AD development by inhibiting ferroptosis in mice [16]. These findings indicate that targeting ferroptosis might alleviate or treat AD. In addition, the immune-inflammatory response was reported to be involved in the progression of STAAD [5]. Several bioinformatic analyses have revealed that the proportion of immune cell infiltration was different between STTAD and healthy controls [17, 18]. Dysregulated ferroptosis is involved in an increasing number of physiological and pathophysiological processes, including immune responses [19]. However, the relationship between ferroptosis and the immune-inflammatory response in STAAD progression is unclear.

Herein, we performed a comprehensive bioinformatics analysis based on weighted gene co-expression network analysis (WGCNA), least absolute shrinkage and selection operator (LASSO), and support vector machine-recursive feature elimination (SVM-RFE) to identify the ferroptosis-associated characteristic genes involved in STAAD, which were expected to serve as diagnostic biomarkers and therapeutic targets. Moreover, we explored the relationship between ferroptosis-associated characteristic genes and immune infiltrating cells to further understand the relationship between ferroptosis and immune-inflammatory response in STAAD progression. Finally, we explored the roles of characteristic genes in pan-cancer analysis to provide new insights into the potential relationship between STAAD and cancer.

Materials and methods

Datasets and data preprocessing

The gene expression profiles of STAAD patients were obtained from GSE52093, GSE98770, and GSE153434 datasets of the Gene Expression Omnibus (GEO) database (https://www.ncbi.nlm.nih.gov/gds/). The GSE52093 dataset included seven STAAD samples and five control samples, which were analyzed using the GPL10558 platform (Illumina HumanHT-12 V4.0 expression beadchip). The GSE153434 dataset included 10 STAAD samples and 10 control samples, which were analyzed using the GPL20795 platform (HiSeq X Ten). The mRNA expression profile of the GSE98770 dataset included six STAAD samples and five control samples, which were analyzed using the GPL14550 platform (Agilent-028004 SurePrint G3 Human GE 8×60K Microarray). The microRNA (miRNA) expression profile of the GSE98770 dataset included six STAAD samples and five control samples, which were analyzed using the GPL17660 platform (Agilent-031181 Unrestricted_Human_miRNA_V16.0_Microarray 030840). After normalization and batch effect correction using "limma" and "sva" R packages, the gene expression profiles of GSE52093 and GSE98770 were merged into a single file as a discovery dataset for subsequent analysis. The GSE153434 were log2-transformed and normalized as a validation dataset using the "limma" R package.

Screening of ferroptosis-associated differentially expressed genes (FDEGs)

The list of ferroptosis-associated genes was extracted from the FerrDb V2 database (http://www.zhounan.org/ferrdb). Using the "limma" R package, FDEGs and differentially expressed miRNAs (DEmiRNAs) were screened using a threshold of $P < 0.05$. The top 50 FDEGs and DEmiRNAs were visualized in a heatmap using the "pheatmap" R package. The significant FDEGs and DEmiRNAs were visualized in the volcano plot using "dplyr", "ggplot2", and "ggrepel" R packages.

Functional enrichment analysis

To gain further insight into the biological functions and pathways of FDEGs, Gene Ontology (GO) enrichment and Kyoto Encyclopedia of Genes and Genomes (KEGG) pathway analyses were performed using the "clusterProfiler", "org.Hs.eg.db", and "enrichplot" R packages. $P < 0.05$ was considered statistically significant. In addition, gene set enrichment analysis (GSEA) was performed based on the gene set "c2.cp.kegg.v7.5.1.symbols.gmt" from the Molecular Signatures Database.

Selection of characteristic genes by WGCNA, LASSO, and SVM-RFE

WGCNA is a comprehensive biological algorithm used for constructing the co-expressed gene modules with high biological significance. The gene co-expression network of ferroptosis-related genes was constructed using the "WGCNA" R package. The "pickSoftTreshold" (WGCNA package) function was used to calculate the soft power β value (range: 1-20) based on the criterion of scale-free network. The adjacency matrix was constructed based on the most appropriate soft power β value. Then, the adjacency matrix was transformed into a topological overlap matrix, and a hierarchical clustering dendrogram was constructed to divide the modules. Finally, the correlation between each module and traits was calculated by Pearson correlation analysis. Then, we identified the most significant module that correlated with STAAD, of which the genes were obtained for subsequent analysis.

LASSO is a regression analysis method used for variable selection and regularization to improve the predictive accuracy and interpretability. The optimal hub genes in STAAD patients were determined by LASSO analysis using the "glmnet" R package.

SVM-RFE is a feature selection algorithm that sorts gene features using sequential backward feature elimination. SVM-RFE was performed to identify the optimal variables by deleting feature vectors using "e1071", "kernlab", and "caret" R packages. The intersection of hub genes obtained by WGCNA, LASSO, SVM-RFE analyses and FDEGs was conducted to determine the overlapped genes using the "VennDiagram" R package. Receiver operating characteristic (ROC) diagnostic curves were constructed and the area under the curve (AUC) was calculated to evaluate the diagnostic accuracy using the "pROC" R package.

Construction of miRNA-mRNA regulatory network

The miRNAs targeted by characteristic genes were predicted using the StarBase database (https://starbase.sysu.edu.cn/). The miRNAs predicted by at least two databases were considered target miRNAs. DEmiRNAs were intersected with target miRNAs to identify the overlapped miRNAs. The miRNA-mRNA regulatory network was constructed using Cytoscape software (version 3.8.2). The top 25 genes interacted with characteristic genes were identified through the STRING interacting network (https://cn.string-db.org/). Then, Bayesian network was constructed to infer the gene regulatory network using the "CBNplot" R packages.

Establishment of a nomogram

A nomogram incorporating the characteristic genes was constructed using the "rms" R package. The diagnostic accuracy and reliability of the nomogram were evaluated using the calibration curve. Decision curve analysis was performed to evaluate the clinical usefulness of the nomogram.

Analysis of immune cell infiltrations

CIBERSORT is a deconvolution algorithm that calculates the relative proportions of 22 types of immune infiltrating cells in tissues. The relative proportions of immune cells in each sample were visualized as a bar plot. The difference in immune cells between STAAD samples and control samples was visualized as a violin plot. The correlations between characteristic genes and immune infiltrating cells were analyzed using Spearman's correlation analysis and visualized as a lollipop plot.

Pan-cancer analysis of characteristic genes

Because ferroptosis is closely associated with various cancers, we used the ferroptosis-associated characteristic genes to explore the potential relationships between cancers and STAAD. We compared the expression of characteristic genes between normal samples and

various cancers, which was visualized in a boxplot. Furthermore, we explored the prognostic value of characteristic genes in pan-cancer analysis using a forest plot. In addition, the correlations between the characteristic genes and immune cells in all The Cancer Genome Atlas (TCGA) cancers were explored using CIBERSORT, EPIC, MCPCOUNTER, QUANTISEQ, TIMER and XCELL algorithms based on the TIMER 2.0 database (http://timer.cistrome.org/).

Drug sensitivity analysis

To develop new drugs to better treat STAAD, drug sensitivity analysis was performed based on the CellMiner database (version 2022.1, database 2.8.1). Pearson correlation analysis between characteristic genes and antitumor drug sensitivity was performed using the "impute", "limma", "ggplot2", and "ggpubr" R packages.

Statistical analysis

The statistical analyses were performed using the Perl software (version 5.32.1.1) and R software (version 4.2.0). Wilcoxon test was used to compare the differences between the two groups. Spearman or Pearson's correlation analysis was used to analyze the correlation between the variables. Cox regression model analysis was used for survival analysis in various cancers. $P < 0.05$ was considered statistically significant.

Results

Data preprocessing and FDEGs screening

After eliminating the batch effects and normalization, GSE52093 and GSE98770 datasets, including 13 STAAD samples and 10 normal samples, were merged into a single gene expression profile for analysis. As shown in **Figure 1A** and **1B**, principal component analysis was performed to evaluate the performance of normalization and batch effect correction. The expression profile of 453 ferroptosis-associated genes was extracted and a total of 65 FDEGs were screened, which included 24 upregulated genes and 41 downregulated genes (Table S1). The top 50 FDEGs were shown in a heatmap (**Figure 1C**), and the FDEGs were visualized as a volcano plot (**Figure 1D**).

GO and KEGG pathway enrichment analyses

The GO function terms comprised biological processes, molecular functions, and cellular components. As expected, the top 10 GO terms were mainly enriched in the cellular responses to chemical stress, iron ion, extracellular stimulus, cellular response to extracellular stimulus, iron ion homeostasis, and transition metal ion homeostasis (**Figure 2A**). The KEGG pathways were mainly enriched in autophagy, ferroptosis, cellular senescence, HIF-1 signaling pathway, mTOR signaling pathway, and NOD-like receptor signaling pathway (**Figure 2B**).

Identification of characteristic genes

First, the most significant module correlated with STAAD was identified using WGCNA. We identified $\beta = 7$ ($R2 = 0.88$) as the most appropriate soft power value to construct the scale-free network (**Figure 3A**). A total of three modules were identified, and their hierarchical clustering dendrogram was constructed (**Figure 3C**). Finally, the correlation between STAAD and modules was shown in a heatmap. The blue module ($cor = 0.53$, $P = 0.009$) was most significantly correlated with STAAD (**Figure 3B**). The 166 genes in the blue module were selected for further analysis. Then, LASSO regression analysis was performed to identify the optimal $\lambda = 0.244$ using ten-fold cross-validation, and the five candidate genes were selected based on the optimal λ (**Figure 3D** and **3E**). Subsequently, SVM-RFE analysis showed a minimum error when the feature number was 8, at which point eight genes were identified as candidate genes (**Figure 3F**). Finally, two characteristic genes (DAZAP1 and GABARAPL2) shared by FDEGs, WGCNA, LASSO, and SVM-RFE were identified using the intersection (**Figure 3G**). Compared with normal samples, we discovered that the expression of DAZAP1 was higher ($P = 5.44e\text{-}04$) but the expression of GABARAPL2 ($P = 9.14e\text{-}04$) was lower in STAAD samples (Table S1).

Validation and evaluation of diagnostic efficacy of characteristic genes in predicting STAAD

In the GSE153434 dataset, we found that DAZAP1 ($P = 3.2e\text{-}04$, **Figure 4A**) was significantly upregulated but GABARAPL2 ($P = 7.6e\text{-}05$, **Figure 4B**) was significantly downregulated in STAAD samples compared with the control

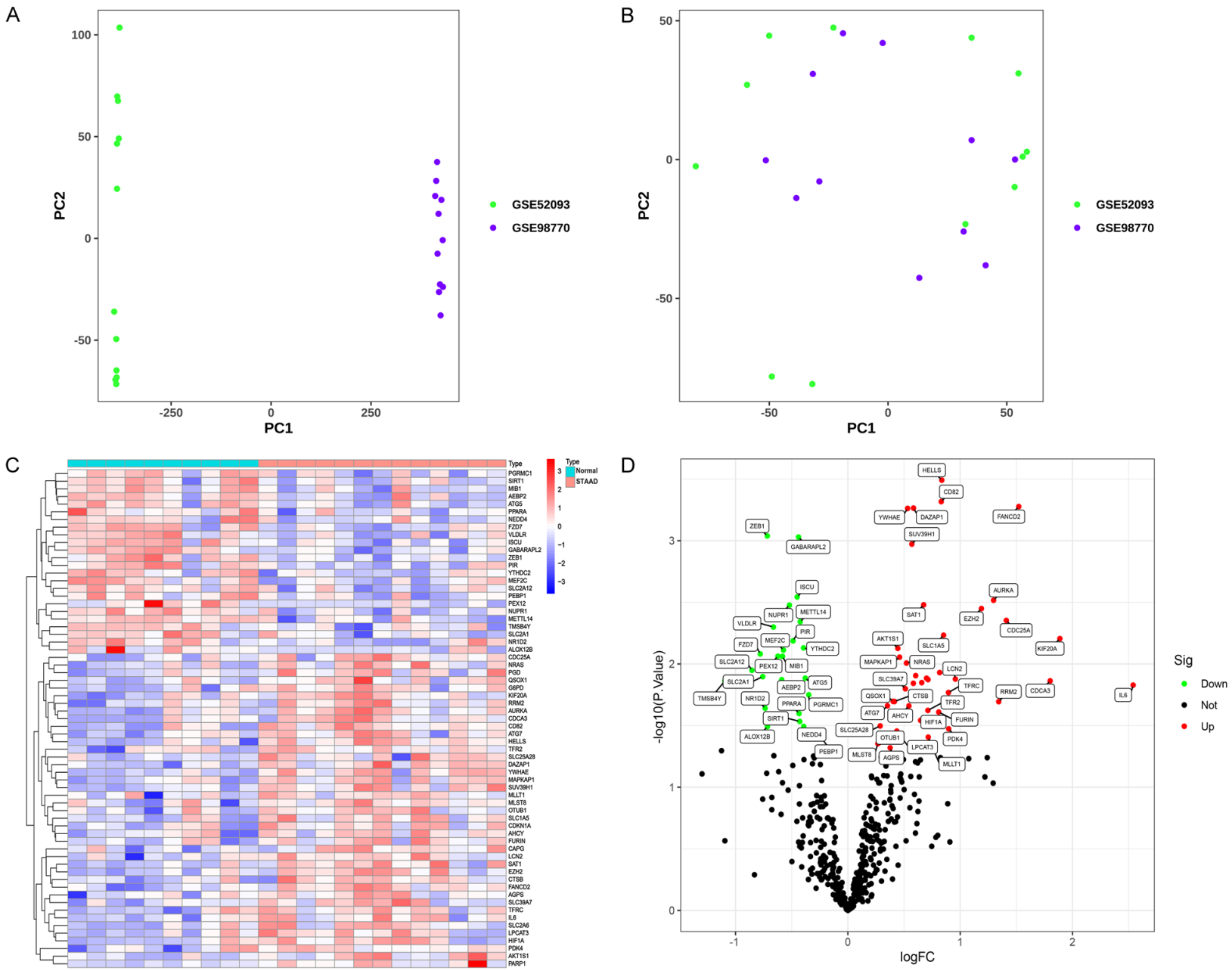
A
PC2
PC1
GSE52093
GSE98770
B
PC2
PC1
GSE52093
GSE98770
C
Type
Normal
STAAD
D
-log10(P.Value)
logFC
Sig
Down
Not
Up

Figure 1. PCA and FDEGs analyses. A. PCA shows the distribution of the two datasets before normalization and batch effect correction. B. PCA shows the distribution of the two datasets after normalization and batch effect correction. C. Heatmap of the top 50 FDEGs between STAAD samples and control samples. The red represents upregulated genes, but the blue represents downregulated genes. D. Volcano plots of FDEGs between STAAD samples and control samples. The red dots represent upregulated genes, the green dots represent downregulated genes and the black dots represent genes with no significant difference. PCA, principal component analysis; FDEGs, ferroptosis-associated differentially expressed genes; STAAD, Stanford type A aortic dissection.

samples, which was consistent with the results of the discovery dataset. Subsequently, ROC diagnostic curves of DAZAP1 and GABARAPL2 were constructed to evaluate the diagnostic efficacy for STAAD. In the discovery dataset, DAZAP1 (AUC: 0.923, 95% confidence interval [CI]: 0.785-1.000; **Figure 4C**) and GABARAPL2 (AUC: 0.900, 95% CI: 0.738-1.000; **Figure 4D**) had a good diagnostic ability for STAAD. In addition, we verified the diagnostic efficacy of characteristic genes in the GSE153434 dataset. ROC curves of DAZAP1 (AUC: 0.940, 95% CI: 0.810-1.000; **Figure 4E**) and GABARAPL2 (AUC: 0.970, 95% CI: 0.880-1.000; **Figure 4F**) showed a robust diagnostic power.

GSEA of characteristic genes

To better illustrate the potential mechanisms of characteristic genes in STAAD, GSEA was performed to compare the biological processes between the low- and high-expression groups that were classified based on the median expressions of characteristic genes. We discovered that the high DAZAP1 expression subgroup was mainly enriched in DNA replication and ribosome, whereas the low DAZAP1 expression subgroup was mainly enriched in bladder cancer, Huntington's disease, oxidative phosphorylation, Parkinson's disease, and proteasome and RIG-I-like receptor signaling pathway (Figure S1A). The high GABARAPL2 expression subgroup was mainly enriched in ABC transporters, gap junctions, tight junctions, tryptophan metabolism, and Wnt signaling pathway, whereas the low GABARAPL2 expression subgroup was mainly enriched in cysteine and methionine metabolism, Parkinson's disease, and Notch signaling pathway (Figure S1B).

miRNA-mRNA regulatory network

After normalization, 183 DEmiRNAs, including 138 upregulated DEmiRNAs and 45 downregulated DEmiRNAs, were identified using the "limma" R package (Figure S2). In total, 46 miRNAs targeted by DAZAP1 and 39 miRNAs targeted by GABARAPL2 were predicted by the StarBase database (Table S2). Based on the negative correlation between miRNA and mRNA, the downregulated DEmiRNAs and upregulated DEmiRNAs were intersected with the miRNAs targeted by DAZAP1 and GABARAPL2, respectively. Finally, two miRNAs (hsa-miR-10b-5p and hsa-miR-199b-5p) targeted by DAZAP1 and seven miRNAs (has-miR-34a-5p, hsa-miR-145-5p, hsa-miR-186-5p, hsa-miR-374a-5p, hsa-miR-374b-5p, hsa-miR-374c-5p, and has-miR-495-3p) targeted by GABARAPL2 were identified to construct the regulatory network using the Cytoscape software (**Figure 5A**).

Furthermore, Bayesian network was constructed to further explore the potential regulatory relationships of DAZAP1 and GABARAPL2 (**Figure 5B**). The regulatory network revealed that DAZAP1 could regulate the expression of ATG4B and TP53INP1, while GABARAPL2 might be involved in the regulation of ATG5, ATG7, and CALCOCO2. In addition, we also discovered that GABARAPL2 might interact with DAZAP1 by targeted ATG5.

Construction of the characteristic gene-based nomogram

A nomogram based on DAZAP1 and GABARAPL2 was constructed as a diagnostic tool for STAAD (**Figure 5C**). The calibration curve demonstrated that the nomogram might be accurate and reliable for diagnosing STAAD (**Figure 5D**). The decision curve analysis further indicated that the nomogram model could provide a robust clinical benefit for patients (**Figure 5E**).

Immune infiltration analysis

The abundances of immune cells in each sample were analyzed using the CIBERSORT algorithm, which was displayed as a bar plot (**Figure 6A**). Furthermore, the violin plot showed that the STAAD group had lower infiltration levels of Tregs and gamma delta T cells, and higher infil-

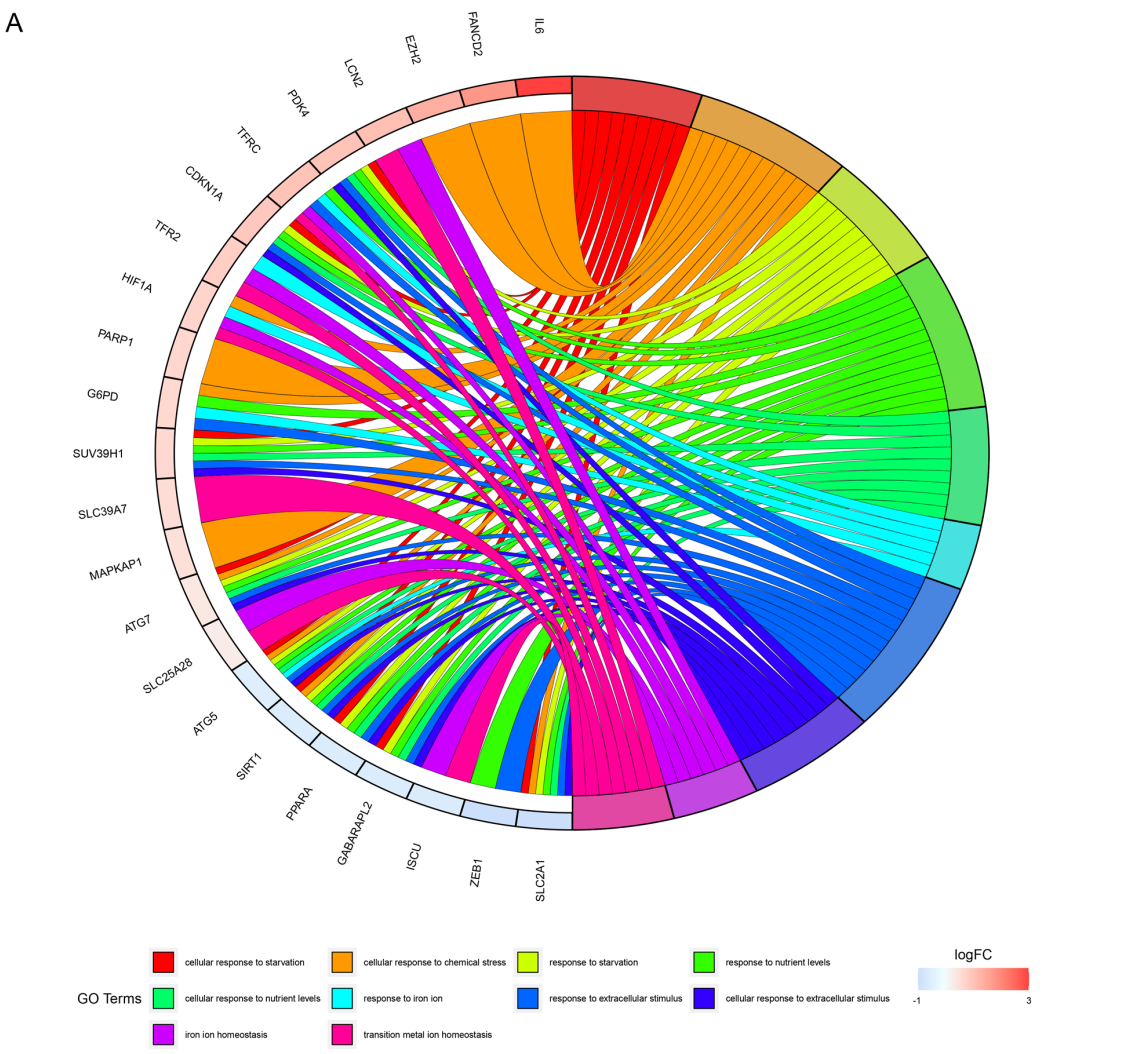
A
IL6
FANCD2
EZH2
LCN2
PDK4
TFRC
CDKN1A
TFR2
HIF1A
PARP1
G6PD
SUV39H1
SLC39A7
MAPKAP1
ATG7
SLC25A28
ATG5
SIRT1
PPARA
GABARAPL2
ISCU
ZEB1
SLC2A1
GO Terms
cellular response to starvation
cellular response to chemical stress
response to starvation
response to nutrient levels
cellular response to nutrient levels
response to iron ion
response to extracellular stimulus
cellular response to extracellular stimulus
iron ion homeostasis
transition metal ion homeostasis
logFC
-1
3

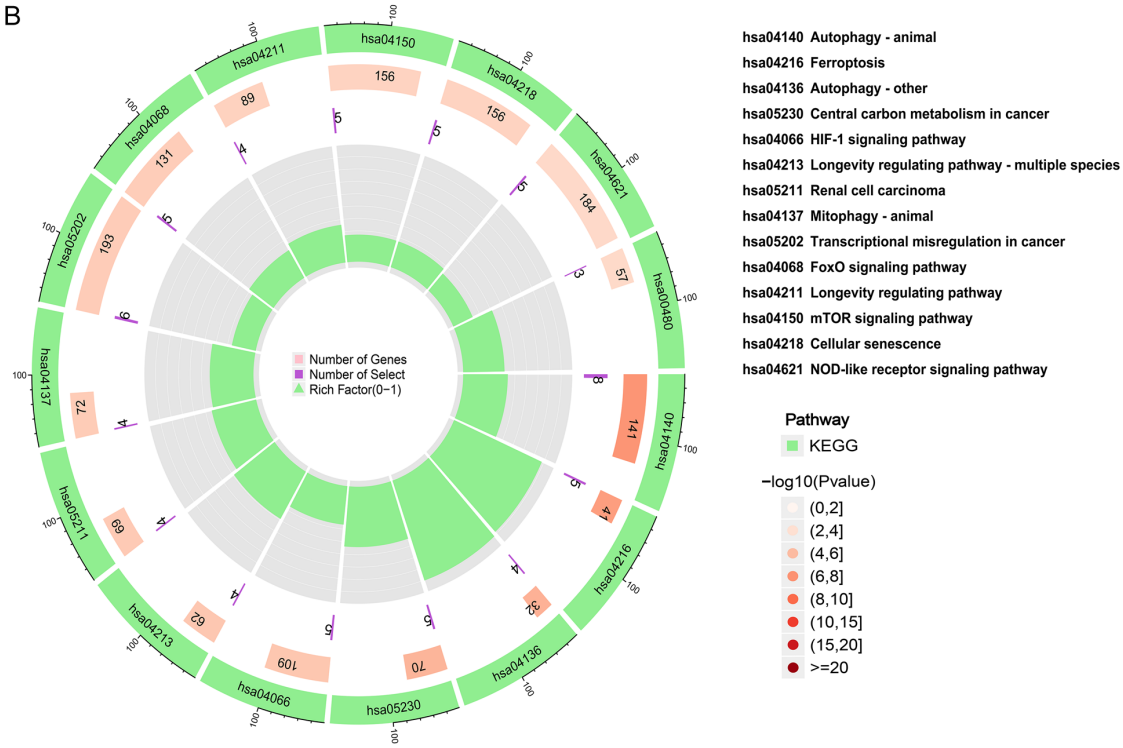
B
hsa04150
hsa04218
hsa04621
hsa00480
hsa04140
hsa04216
hsa04136
hsa05230
hsa04066
hsa04213
hsa05211
hsa04137
hsa05202
hsa04068
hsa04211
156
156
184
57
141
32
70
109
62
69
72
193
131
89
Number of Genes
Number of Select
Rich Factor(0-1)
hsa04140 Autophagy - animal
hsa04216 Ferroptosis
hsa04136 Autophagy - other
hsa05230 Central carbon metabolism in cancer
hsa04066 HIF-1 signaling pathway
hsa04213 Longevity regulating pathway - multiple species
hsa05211 Renal cell carcinoma
hsa04137 Mitophagy - animal
hsa05202 Transcriptional misregulation in cancer
hsa04068 FoxO signaling pathway
hsa04211 Longevity regulating pathway
hsa04150 mTOR signaling pathway
hsa04218 Cellular senescence
hsa04621 NOD-like receptor signaling pathway
Pathway
KEGG
−log10(Pvalue)
(0,2]
(2,4]
(4,6]
(6,8]
(8,10]
(10,15]
(15,20]
>=20

Figure 2. Functional enrichment analysis of FDEGs. A. GO enrichment analysis. B. KEGG enrichment analysis. FDEGs, ferroptosis-associated differentially expressed genes; GO, Gene Ontology; KEGG, Kyoto Encyclopedia of Genes and Genomes.

tration levels of resting NK cells and monocytes, compared with the control group (**Figure 6B**). Moreover, the correlation of the two characteristic genes with immune infiltration cells was explored. We found that DAZAP1 was positively correlated with resting NK cells, monocytes, and memory B cells, but negatively correlated with gamma delta T cells (**Figure 7A**). GABARAPL2 was positively correlated with CD8 T cells, gamma delta T cells, and Tfh cells, while it was negatively correlated with resting NK cells and monocytes (**Figure 7B**).

Pan-cancer analysis of DAZAP1 and GABARAPL2

Based on the TCGA data, differential analysis showed that the expression of DAZAP1 was high in BLCA, BRCA, CESC, CHOL, COAD, DLBC, HNSC, KICH, KIRC, KIRP, LIHC, LUAD, LUSC, PRAD, READ, STAD, THCA, and UCEC, while the expression of GABARAPL2 was low in BRCA, CESC, COAD, KICH, KIRC, LUAD, LUSC, READ, and UCEC (**Figure 8A** and **8B**). Furthermore, we explored the correlation between DAZAP1/GABARAPL2 and prognosis, including overall survival (OS) and progression-free survival (PFS) based on the TCGA data. Univariate cox regression analysis for OS revealed that DAZAP1 expression was significantly associated with OS in 10 cancers: ACC, KIRC, LGG, LIHC, MESO, and SARC as a risk factor, whereas BLCA, READ, STAD, and THYM as a protective factor (**Figure 9A**). GABARAPL2 expression was significantly associated with OS in 11 cancers: ACC, KICH, KIRC, LGG, MESO, PAAD, and SKCM as a protective factor, whereas BRCA, ESCA, HNSC, and STAD as a risk factor (**Figure 9B**). Univariate cox regression analysis for PFS revealed that DAZAP1 expression was significantly associated with PFS in seven cancers as a risk factor in ACC, KIRC, LGG, LIHC, PCPG, PRAD, and SARC (**Figure 9C**). GABARAPL2 expression was significantly associated with PFS in seven cancers a as protective factor in KICH, KIRC, LGG, and PAAD, and a risk factor in ESCA, HNSC, and STAD (**Figure 9D**).

Furthermore, pan-cancer analysis of immune cell infiltration using CIBERSORT, EPIC, MCPCOUNTER, QUANTISEQ, TIMER and XCELL algorithms showed that different immune cells such as CD8+ T cell, CD4+ T cell, macrophages, neutrophil and B cells were strongly correlated with DAZAP1 (**Figure 10**) and GABARAPL2 (**Figure 11**) in various cancers.

Correlation between characteristic genes and drug sensitivity

The drug sensitivity analysis showed that DAZAP1 and GABARAPL2 were significantly associated with the sensitivity of various anticancer drugs (**Figure 12**). DAZAP1 was positively correlated with some drugs, including nelarabine, hydroxyurea, and cladribine, but negatively correlated with depsipeptide and ARRY-162. GABARAPL2 was positively correlated with LEE-011, palbociclib, and ifosfamide.

Discussion

AD is a devastating disease with a high mortality rate, which is characterized by tears in the aortic wall [17]. Poorly controlled hypertension, inherited connective tissue lesions, vascular inflammation, history of cardiac surgery, and trauma are the primary pathological causes of aortic wall damage and contribute to AD [20-22]. The increased oxidative stress and expression of inflammatory factors and matrix metalloproteinases caused by immune cell infiltration in the aortic wall contribute to vascular SMC apoptosis and aortic remodeling, which play a crucial role in AD pathogenesis [10]. However, the identification of potential molecular pathways underlying STAAD is difficult. Ferroptosis, a recently identified form of regulated cell death, is distinct from apoptosis, autophagy, pyroptosis, and necroptosis. It plays a critical role in regulating immune cell function [23]. Ferroptosis is closely associated with the biological processes of cancers, blood diseases, ischemia-reperfusion injury, and cardiovascular diseases [24-27]. Recent studies have shown that glutathione peroxidase 4, glutathione, and iron accumulation play critical roles in cardiovascular diseases [28, 29]. Nonetheless, studies of the ferroptosis-associated biomarkers and pathways in the progression of STAAD are scarce.

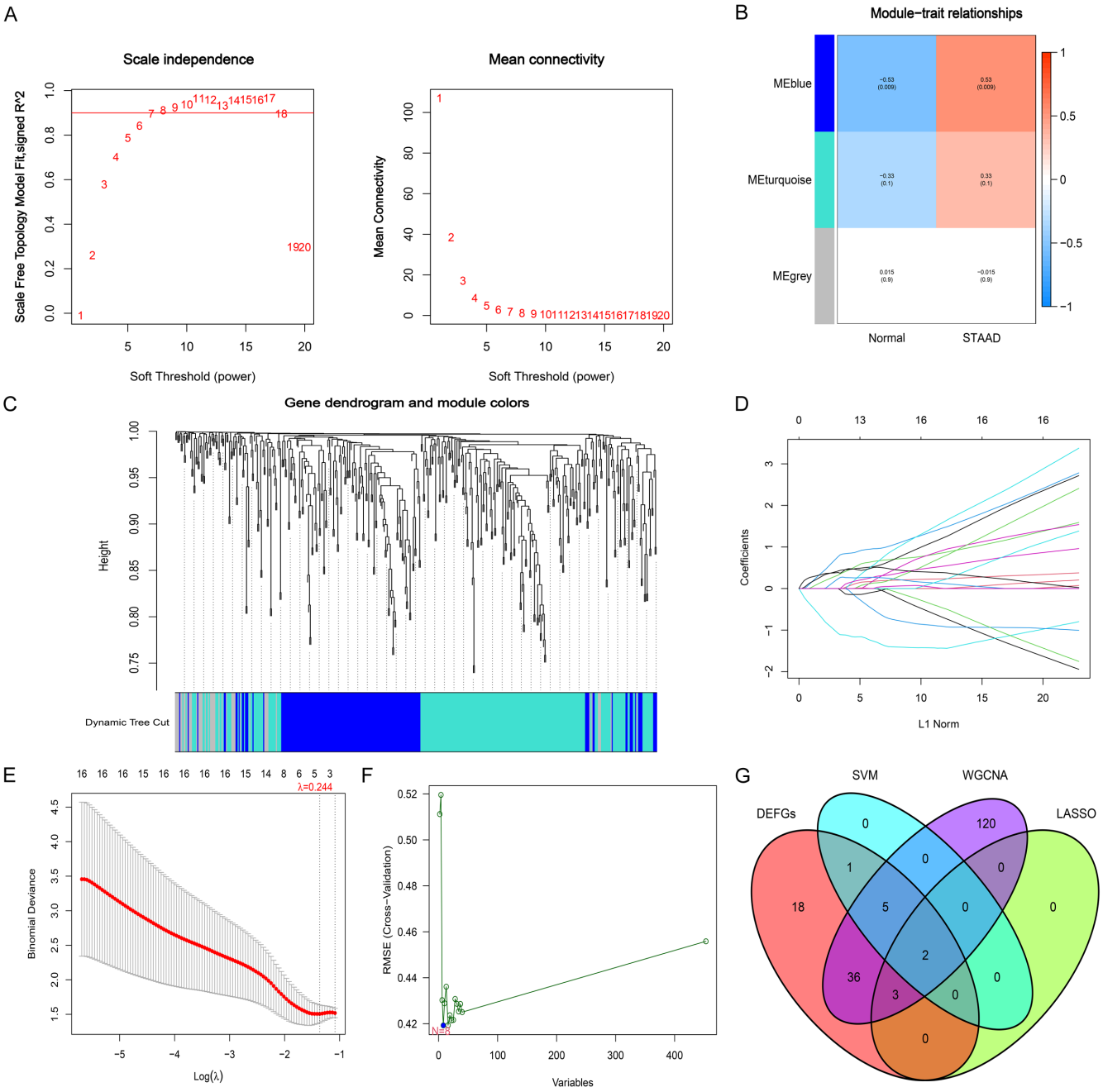
A
Scale independence
Scale Free Topology Model Fit,signed R^2
Soft Threshold (power)
Mean connectivity
Mean Connectivity
Soft Threshold (power)
B
Module−trait relationships
MEblue
MEturquoise
MEgrey
Normal
STAAD
C
Gene dendrogram and module colors
Height
Dynamic Tree Cut
D
Coefficients
L1 Norm
E
Binomial Deviance
Log(λ)
λ=0.244
F
RMSE (Cross−Validation)
Variables
N=8
G
DEFGs
SVM
WGCNA
LASSO

Figure 3. Construction of WGCNA co-expression network and identification of characteristic genes by LASSO and SVM-RFE. A. Determination of most appropriate soft power β value. B. Heatmap of correlation between modules and occurrence of STAAD. C. Gene co-expression modules represented by different colors under the clustering dendrogram. D, E. Identification of the optimal λ and selection of candidate genes in the LASSO model. F. Identification of candidate genes by SVM-RFE algorithm. G. Venn diagram of the characteristic genes shared by FDEGs, WGCNA, LASSO, and SVM-RFE. WGCNA, weighted gene co-expression network analysis; LASSO, least absolute shrinkage and selection operator; SVM-RFE, support vector machine-recursive feature elimination; STAAD, Stanford type A aortic dissection; FDEGs, ferroptosis-associated differentially expressed genes.

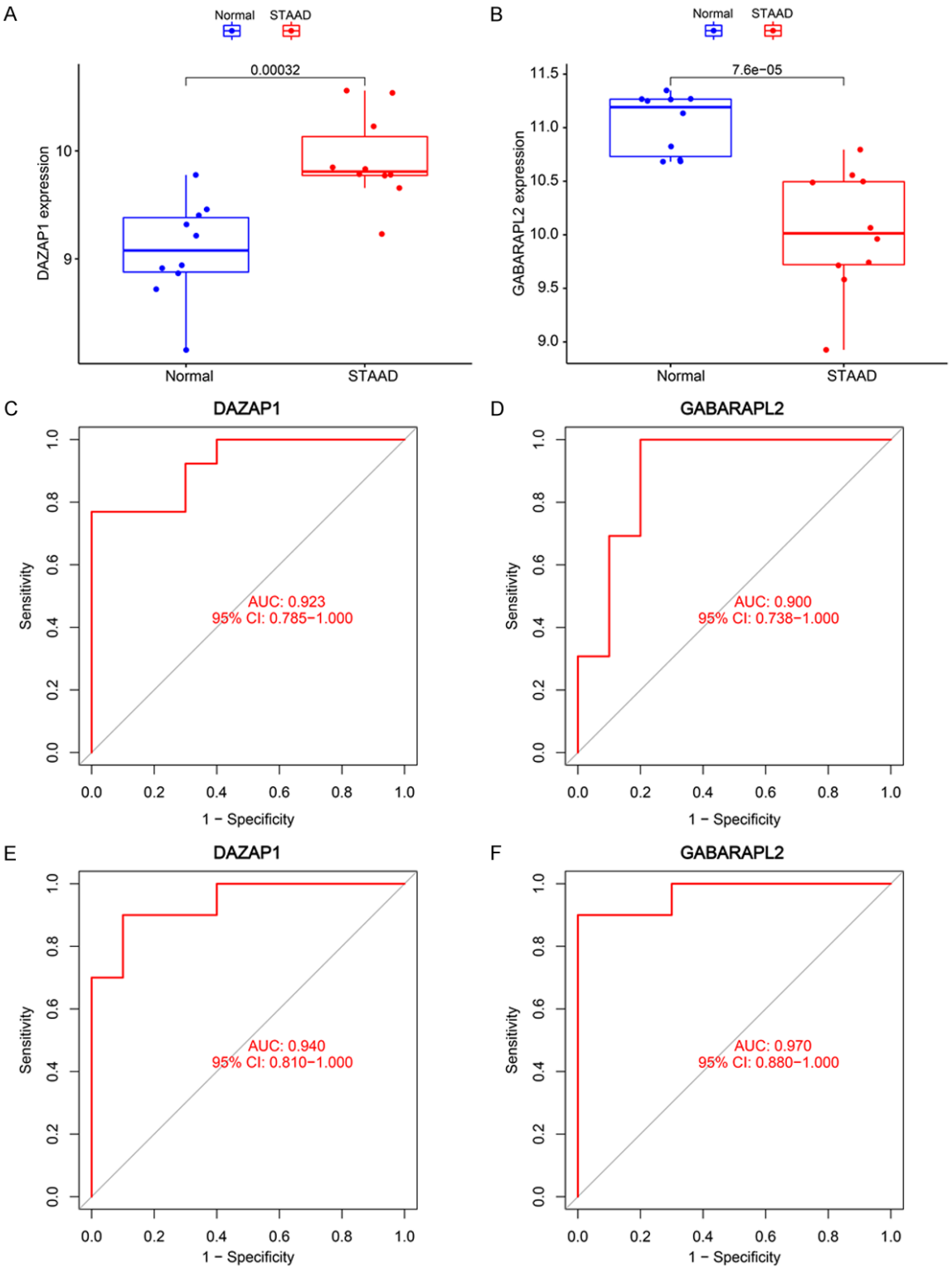

Figure 4. Validation and evaluation of expression and diagnostic efficacy of characteristic genes. A, B. Comparison of DAZAP1 and GABARAPL2 expression between control samples and STAAD samples in the GSE153434 dataset. C, D. ROC diagnostic curves of DAZAP1 and GABARAPL2 in discovery dataset. E, F. ROC diagnostic curves of DAZAP1 and GABARAPL2 in the GSE153434 dataset. STAAD, Stanford type A aortic dissection; ROC, receiver operating characteristic.

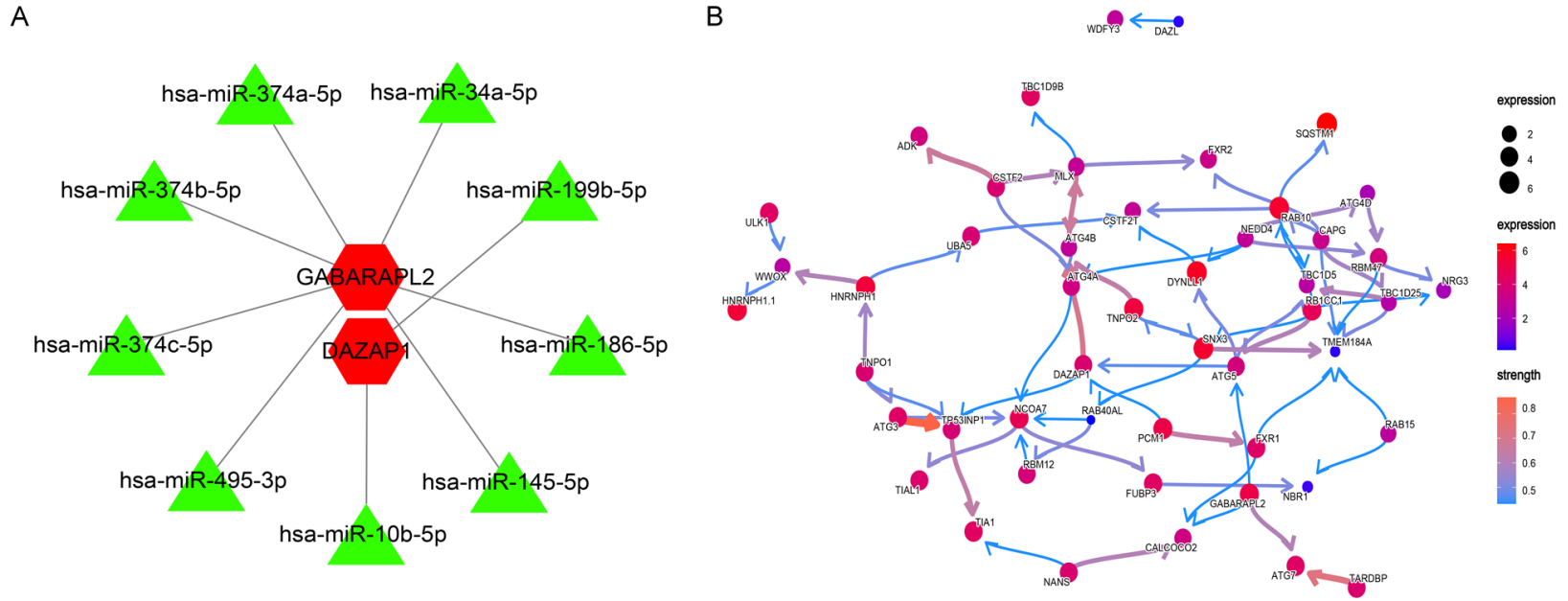

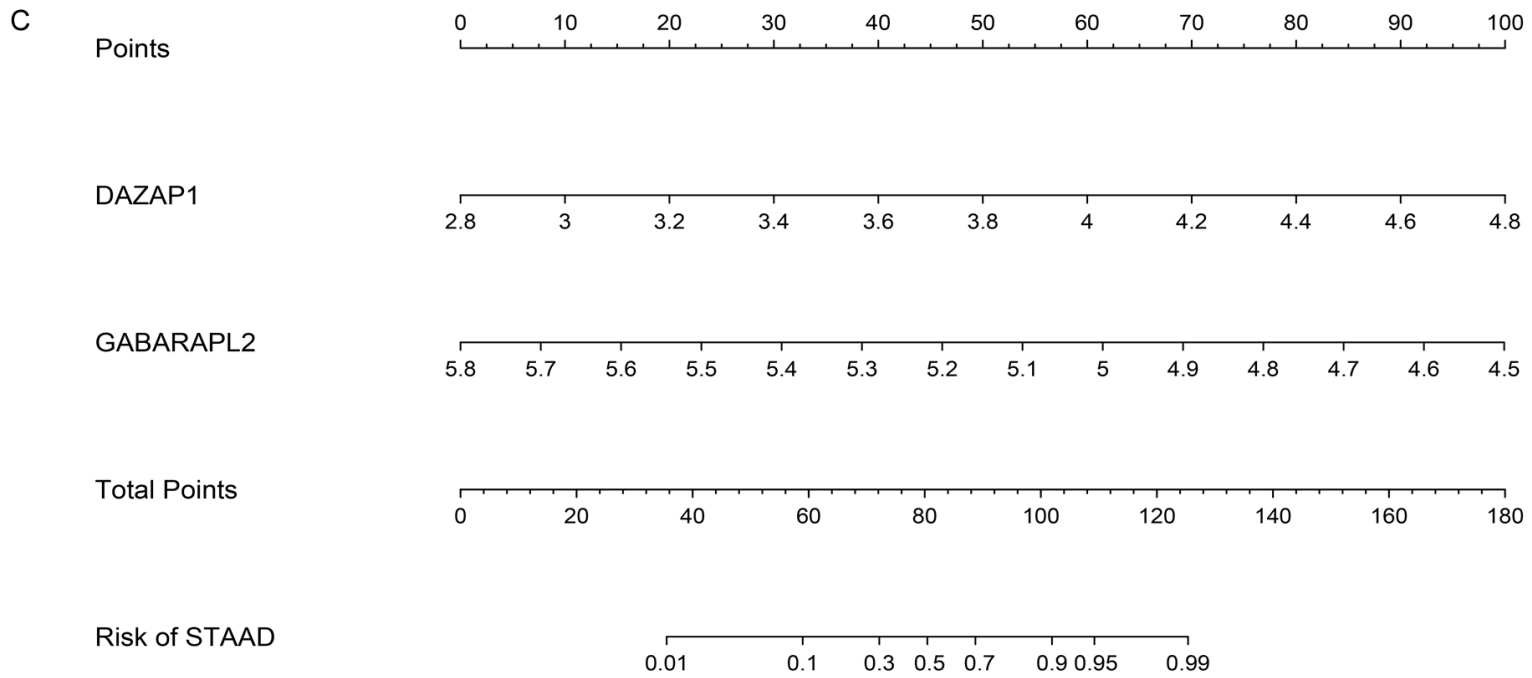
C
Points
0 10 20 30 40 50 60 70 80 90 100
DAZAP1
2.8 3 3.2 3.4 3.6 3.8 4 4.2 4.4 4.6 4.8
GABARAPL2
5.8 5.7 5.6 5.5 5.4 5.3 5.2 5.1 5 4.9 4.8 4.7 4.6 4.5
Total Points
0 20 40 60 80 100 120 140 160 180
Risk of STAAD
0.01 0.1 0.3 0.5 0.7 0.9 0.95 0.99

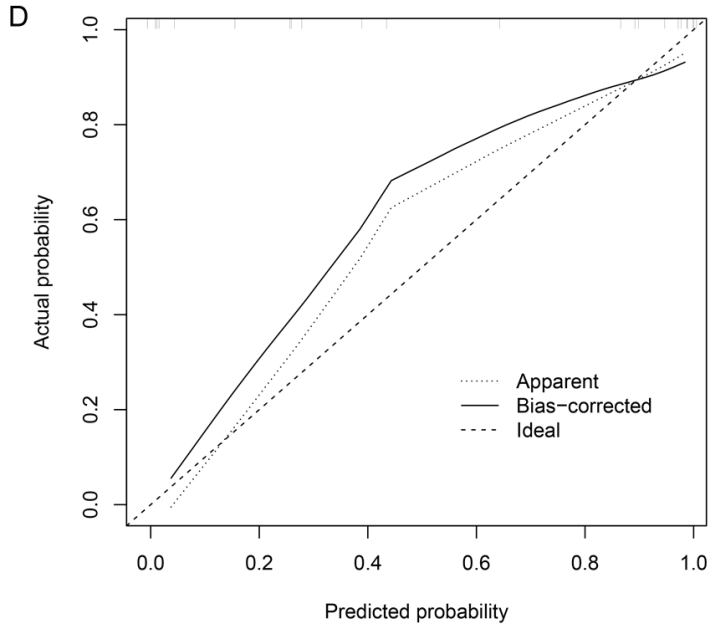
D
Actual probability
0.0 0.2 0.4 0.6 0.8 1.0
Predicted probability
0.0 0.2 0.4 0.6 0.8 1.0
Apparent
Bias−corrected
Ideal

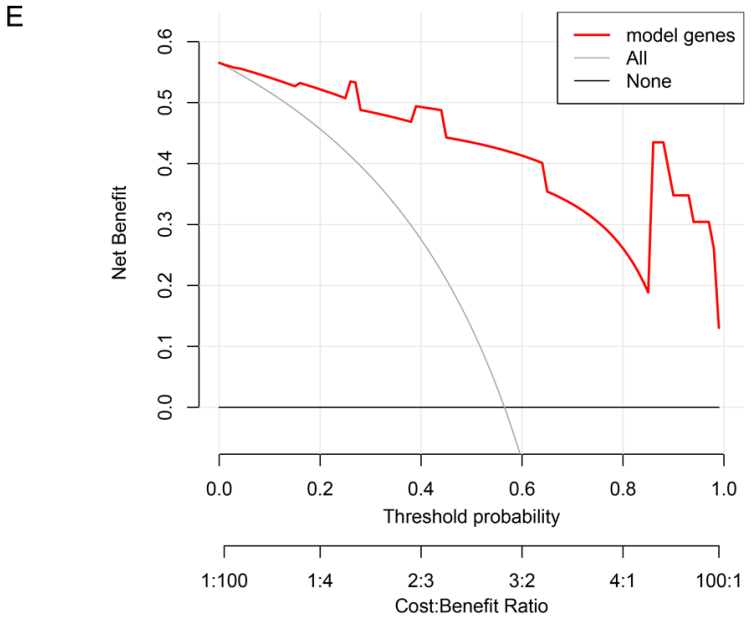
E
Net Benefit
0.0 0.1 0.2 0.3 0.4 0.5 0.6
model genes
All
None
0.0 0.2 0.4 0.6 0.8 1.0
Threshold probability
1:100 1:4 2:3 3:2 4:1 100:1
Cost:Benefit Ratio

Figure 5. A. A miRNA-mRNA regulatory network based on DAZAP1 and GABARAPL2. B. Bayesian regulatory network of DAZAP1 and GABARAPL2. C. A nomogram based on DAZAP1 and GABARAPL2. D. The calibration curve of the nomogram. E. The decision curve analysis of the nomogram. miRNA, microRNA; STAAD, Stanford type A aortic dissection.

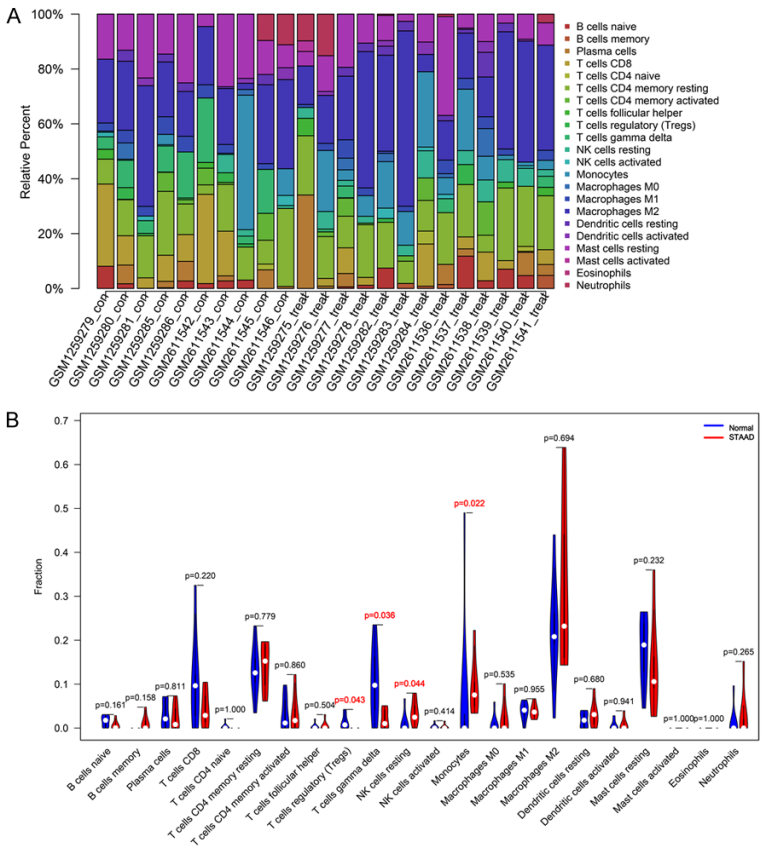

Figure 6. Immune infiltration analysis. A. The abundance of 22 types of immune cells in each sample evaluated by CIBERSORT algorithm. B. The differences in immune cells between control samples and STAAD samples. STAAD, Stanford type A aortic dissection.

Herein, we screened 24 upregulated and 41 downregulated ferroptosis-associated genes in STAAD compared with the control samples. Subsequently, GO and KEGG enrichment analyses showed that the FDEGs were mainly enriched in pathways highly associated with ferroptosis and immune-inflammatory responses. On the basis of WGCNA, SVM-REF, and LASSO regression analyses, upregulated DAZAP1 and downregulated GABARAPL2 were identified as characteristic genes. ROC analysis revealed that both of them were helpful for the early diagnosis of STAAD.

DAZAP1, which is a widely and abundantly expressed RNA-binding protein, plays a critical role in posttranscriptional modifications, including alternative splicing, nucleocytoplasmic transport, and translation [30-32]. Huang et al. found that DAZAP1 was significantly upregulated in synovitis of osteoarthritis by bioinformatics analysis [33]. Wang et al. revealed that higher expression of DAZAP1 was significantly correlated with larger tumor size, higher incidence of vascular invasion, and worse prognosis in hepatocellular carcinoma [34]. Meanwhile, DAZAP1 could regulate ferroptosis in hepatocellular carcinoma cells by targeting SLC7A11 [34]. GABARAPL2, which was initially identified for its involvement in protein transport and membrane fusion events, is best recognized for its role in autophagy [35]. Emerging evidence indicates that high mRNA expression of GABARAPL2 was associated with better OS in renal cancer but worse OS in head and neck cancer [36]. In mice, excessive activation of caspase-11 inflammasomes and a destructive immune response were caused by a lack of GABARAPL2 [37, 38]. A bioinformatics analysis revealed that GABARAPL2 is one of the ferroptosis-associated hub genes in sepsis and had a robust diagnosis power for sepsis [39]. However, no previous studies have reported the potential roles of DAZAP1 and GABARAPL2 in the field of STAAD. Our study is the first to suggest that dysregulation of DAZAP1 and GABARAPL2 may play crucial roles in STAAD progression.

MiRNAs negatively regulate the expression of protein-coding genes through direct binding to the target mRNAs [40]. Previous studies have confirmed that miRNAs play an important role in cardiovascular diseases [41]. Our miRNA-

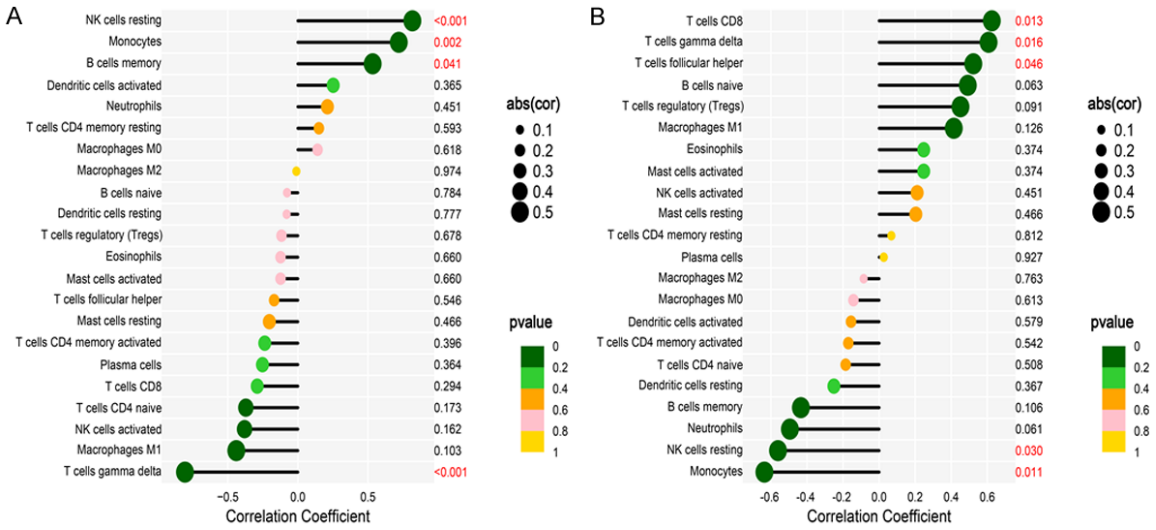

Figure 7. The correlation between (A) DAZAP1, (B) GABARAPL2 and immune infiltrating cells.

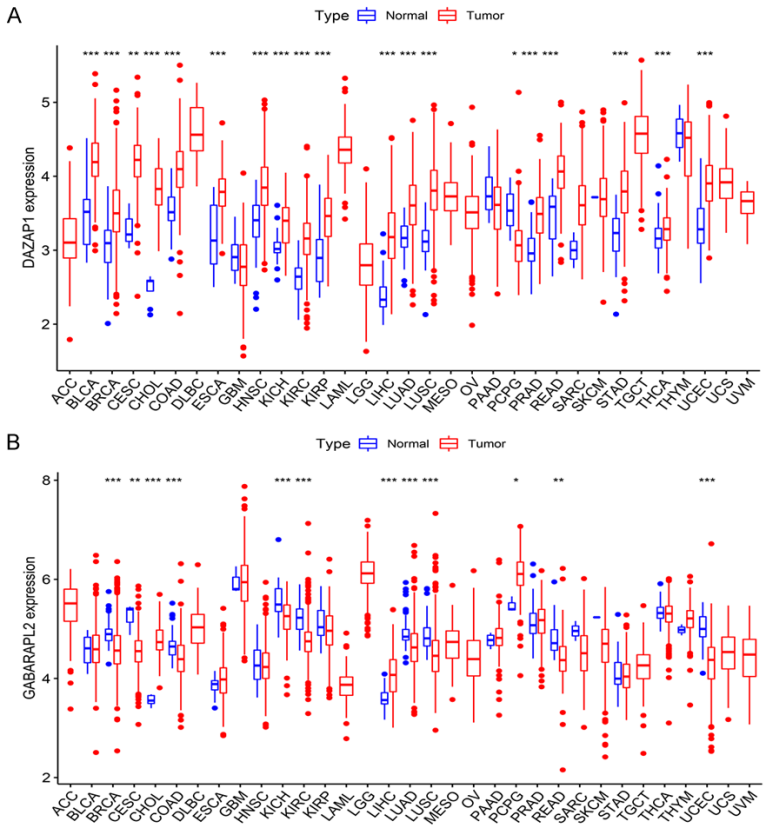

Figure 8. The expression of characteristic genes in pan-cancer analysis. Pancaner expression levels of (A) DAZAP1 and (B) GABARAPL2 in the TCGA dataset (*P < 0.05, **P < 0.01, ***P < 0.001). TCGA, The Cancer Genome Atlas.

mRNA regulatory network indicated that dysregulation of DAZAP1 and GABARAPL2 in STAAD might be regulated by miRNAs. Furthermore, GSEA showed that DAZAP1 was associated with DNA replication, oxidative phosphorylation, and RIG-I-like receptor signaling pathway, while GABARAPL2 was associated with ABC transporters, Notch signaling pathway, and Wnt signaling pathway. For example, iron plays a critical role in many cellular functions, including DNA replication and repair [42]. Jang et al. revealed that suppression of oxidative phosphorylation could significantly aggravate RSL3-induced ferroptosis in cardiomyocytes [43]. The activation of the Wnt/β-catenin signaling pathway leads to weakened cellular lipid ROS production, thereby suppressing ferroptosis in gastric cancer cells [44]. Shan et al. discovered that the potential mechanism of heme-induced ferroptosis in human nucleus pulposus cells might involve the Notch signaling pathway [45]. Hence, we speculated that DAZAP1 and GABARAPL2 might be involved in STAAD progression through these ferroptosis-related pathways.

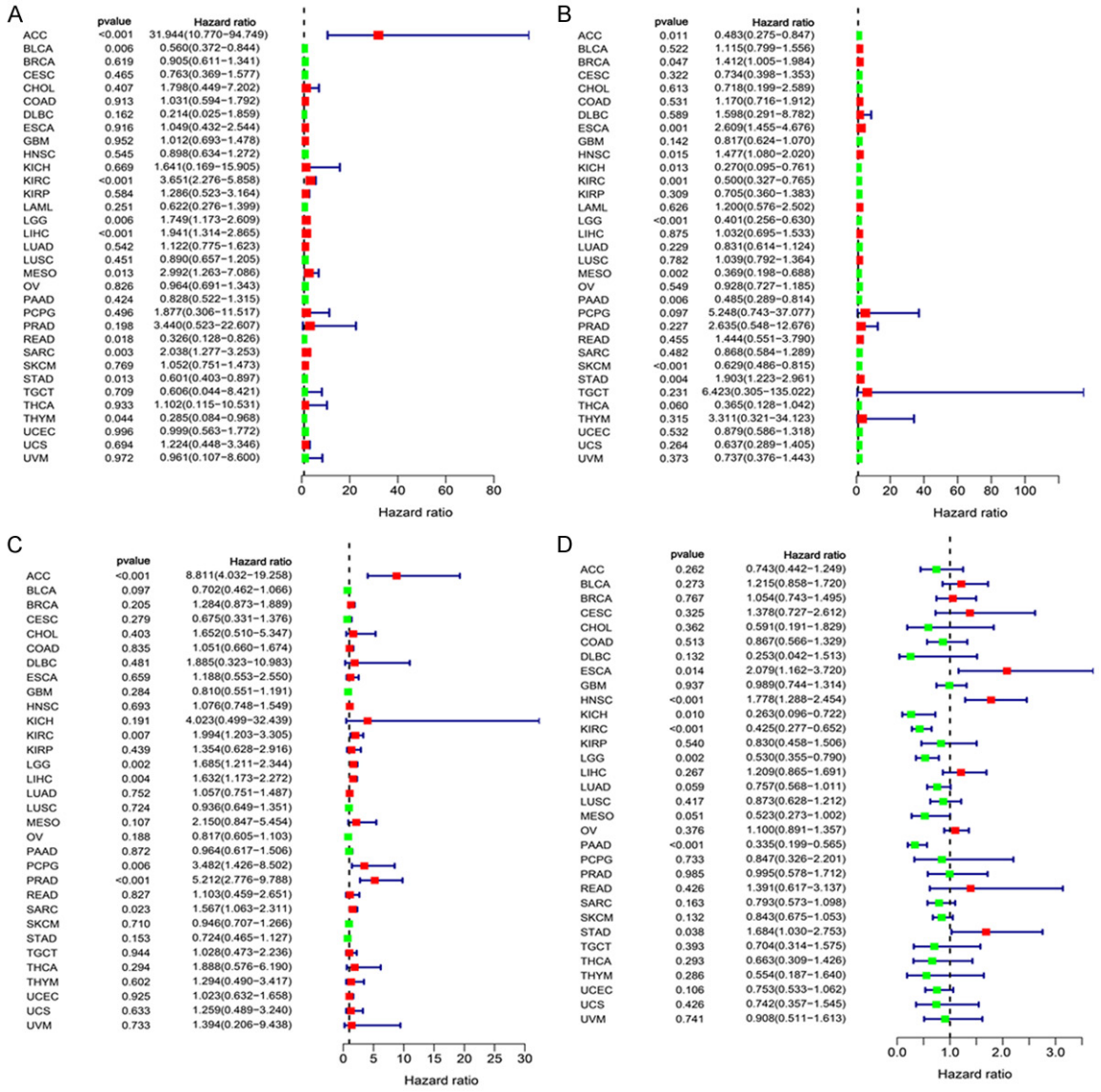

Figure 9. The correlation between characteristic genes and prognosis in pan-cancer. Univariate cox regression analysis of the correlation between (A) DAZAP1 and (B) GABARAPL2 expression and OS in various tumors. Univariate cox regression analysis of the correlation between (C) DAZAP1 and (D) GABARAPL2 expression and PFS in various tumors. Red represents a risk factor and green represents a protective factor. OS, overall survival; PFS, progression-free survival.

Accumulating evidence suggests that dysregulation of monocytes is closely associated with STAAD progression [46-49]. Li et al. revealed that a specific decrease in monocytes and macrophages significantly prevented AD occurrence [50]. Shen et al. revealed that the level of M2-like monocytes was downregulated, indicating that monocytes are prone to the inflammatory response in STAAD [51]. They also found that monocyte-derived proBDNF was involved in the inflammatory response in STAAD progression [51]. Besides, macrophages were found to play a crucial role in STAAD [47, 52]. However, Liu et al. revealed that expanded macrophages originated primarily from circulating monocytes in AD [53]. Herein, immune infiltration analysis suggested that monocytes were higher in the STAAD group compared with the control group, indicating that monocytes might play a major role in the immune-inflammatory response of STAAD. Ferroptosis plays a critical role in regulating immune cell function. On the one hand, ferroptosis of immune cells could affect the number and function of

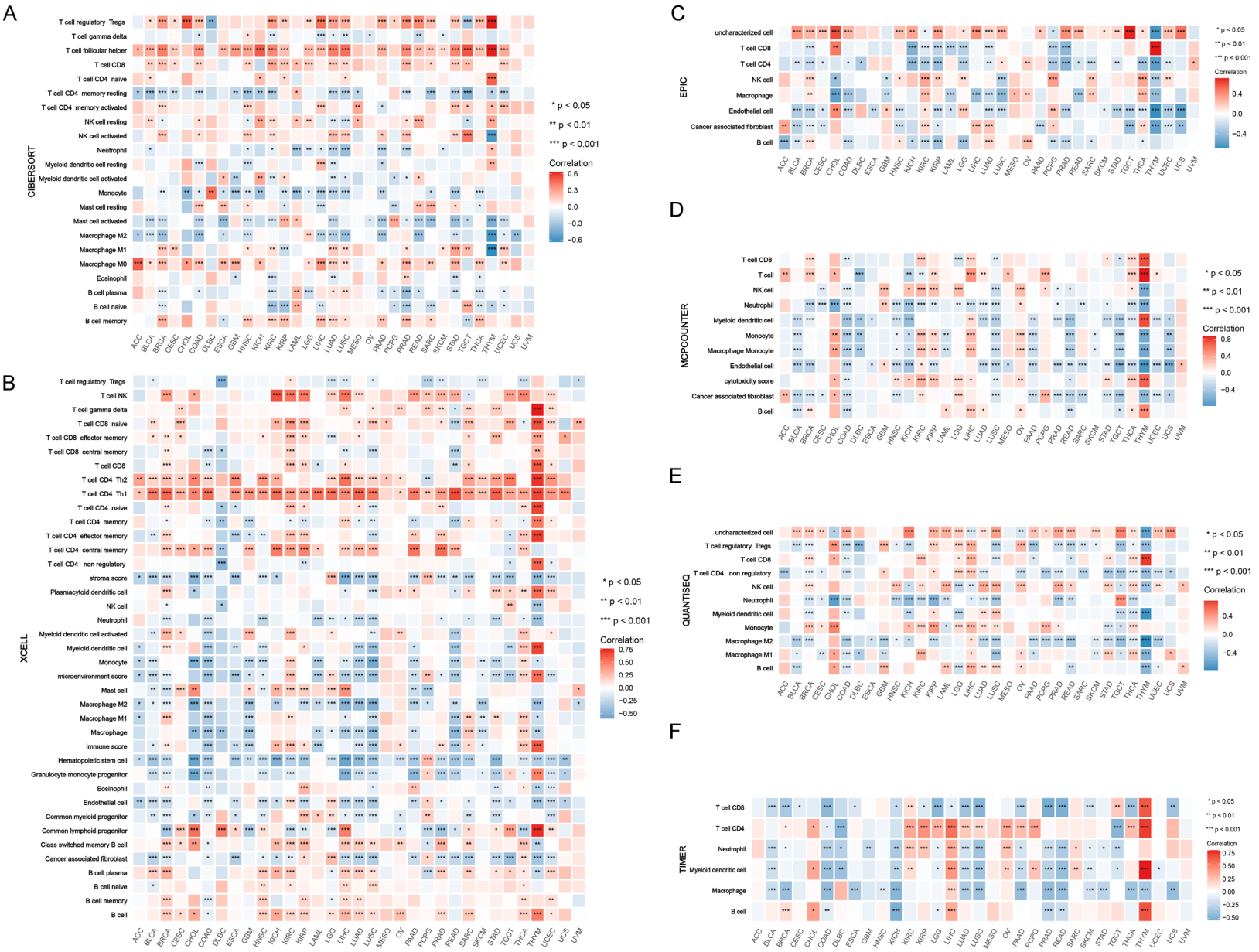
A
CIBERSORT
T cell regulatory Tregs
T cell gamma delta
T cell follicular helper
T cell CD8
T cell CD4 naive
T cell CD4 memory resting
T cell CD4 memory activated
NK cell resting
NK cell activated
Neutrophil
Myeloid dendritic cell resting
Myeloid dendritic cell activated
Monocyte
Mast cell resting
Mast cell activated
Macrophage M2
Macrophage M1
Macrophage M0
Eosinophil
B cell plasma
B cell naive
B cell memory
B
XCELL
T cell regulatory Tregs
T cell NK
T cell gamma delta
T cell CD8 naive
T cell CD8 effector memory
T cell CD8 central memory
T cell CD8
T cell CD4 Th2
T cell CD4 Th1
T cell CD4 naive
T cell CD4 memory
T cell CD4 effector memory
T cell CD4 central memory
T cell CD4 non regulatory
stroma score
Plasmacytoid dendritic cell
NK cell
Neutrophil
Myeloid dendritic cell activated
Myeloid dendritic cell
Monocyte
microenvironment score
Mast cell
Macrophage M2
Macrophage M1
Macrophage
immune score
Hematopoietic stem cell
Granulocyte monocyte progenitor
Eosinophil
Endothelial cell
Common myeloid progenitor
Common lymphoid progenitor
Class switched memory B cell
Cancer associated fibroblast
B cell plasma
B cell naive
B cell memory
B cell
ACC BLCA BRCA CESC CHOL COAD DLBC ESCA GBM HNSC KICH KIRC KIRP LAML LGG LIHC LUAD LUSC MESO OV PAAD PCPG PRAD READ SARC SKCM STAD TGCT THCA THYM UCEC UCS UVM
* p < 0.05
** p < 0.01
*** p < 0.001
Correlation
C
EPIC
uncharacterized cell
T cell CD8
T cell CD4
NK cell
Macrophage
Endothelial cell
Cancer associated fibroblast
B cell
D
MCPCOUNTER
T cell CD8
T cell
NK cell
Neutrophil
Myeloid dendritic cell
Monocyte
Macrophage Monocyte
Endothelial cell
cytotoxicity score
Cancer associated fibroblast
B cell
E
QUANTISEQ
uncharacterized cell
T cell regulatory Tregs
T cell CD8
T cell CD4 non regulatory
NK cell
Neutrophil
Myeloid dendritic cell
Monocyte
Macrophage M2
Macrophage M1
B cell
F
TIMER
T cell CD8
T cell CD4
Neutrophil
Myeloid dendritic cell
Macrophage
B cell

Figure 10. The correlation between DAZAP1 and immune cells in all TCGA cancers by CIBERSORT (A), XCELL (B), EPIC (C), MCPCOUNTER (D), QUANTISEQ (E) and TIMER (F) algorithms. TCGA, The Cancer Genome Atlas.

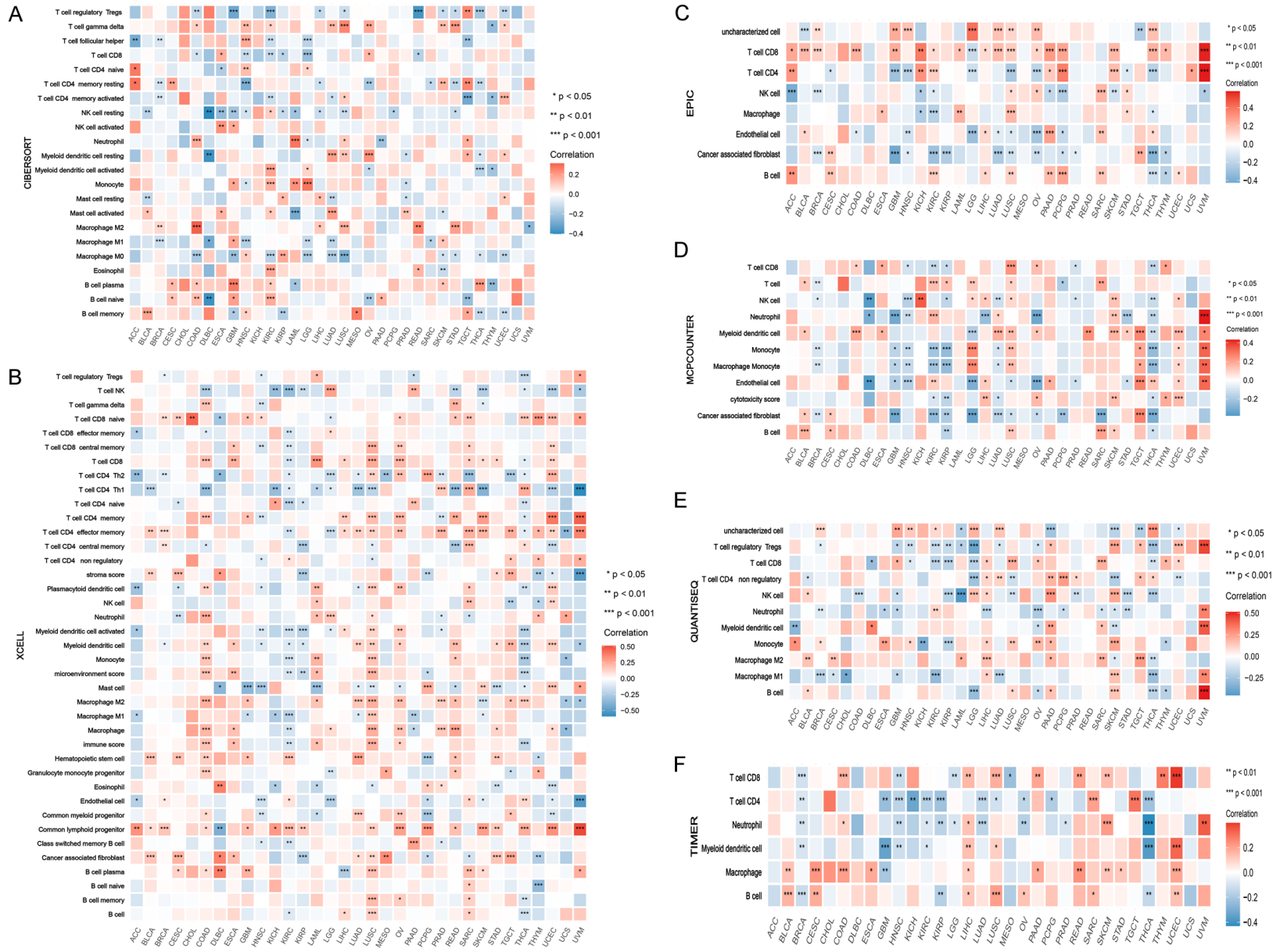

Figure 11. The correlation between GABARAPL2 and immune cells in all TCGA cancers by CIBERSORT (A), XCELL (B), EPIC (C), MCPCOUNTER (D), QUANTISEQ (E) and TIMER (F) algorithms. TCGA, The Cancer Genome Atlas.

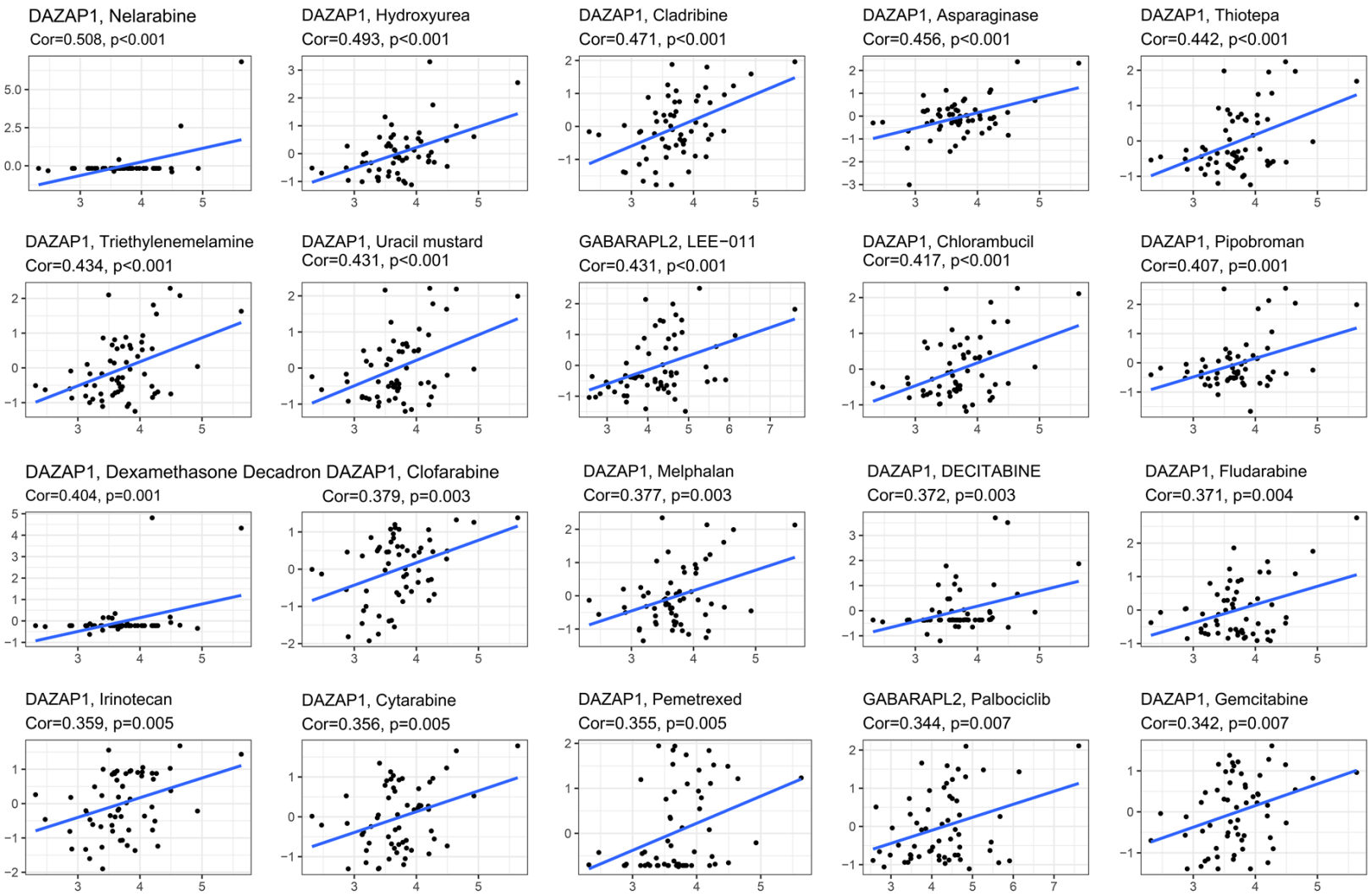

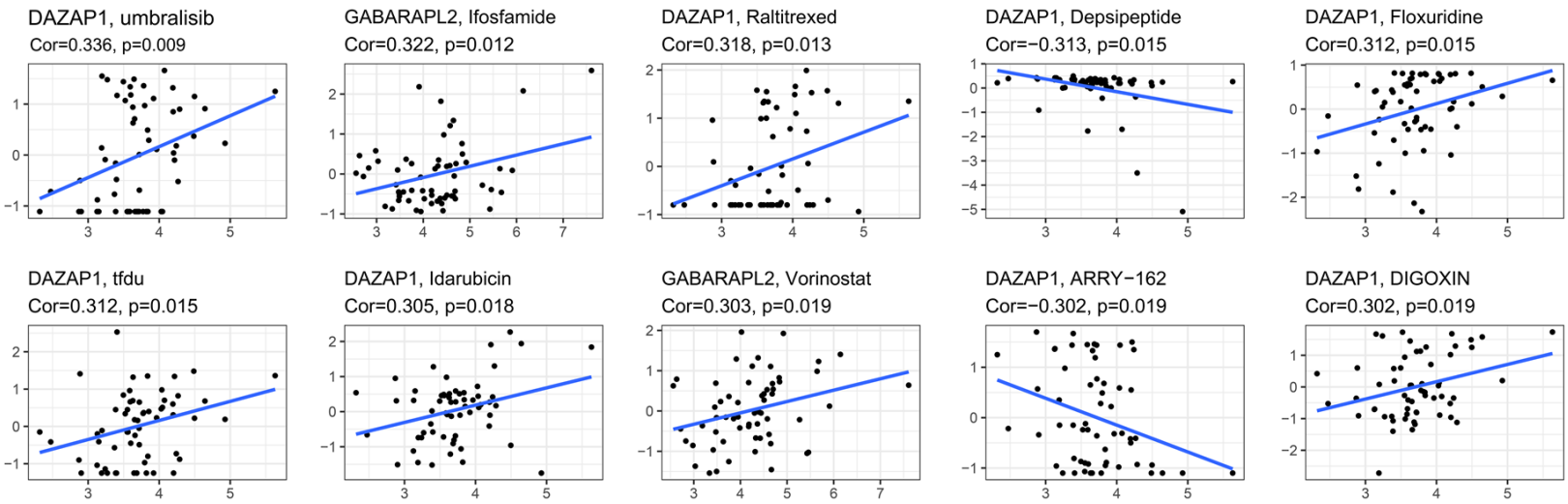

Figure 12. Drug sensitivity analysis of DAZAP1 and GABARAPL2 with various antitumor drugs.

immune cells [19]. On the other hand, ferroptosis of non-immune cells could also be recognized by immune cells, thereby initiating a range of immune-inflammatory responses [19]. In our study, upregulated DAZAP1 was positively correlated with monocytes, whereas downregulated GABARAPL2 was negatively correlated with monocytes. Consequently, we supposed that DAZAP1 and GABARAPL2 might contribute to STAAD progression via the immune-inflammatory response activated by monocytes. Furthermore, Bayesian network revealed that DAZAP1 could regulate the expression of ATG4B and TP53INP1, while GABARAPL2 might be involved in the regulation of ATG5, ATG7, and CALCOCO2. Previous studies have demonstrated that ATG4B, ATG5, ATG7 and TP53INP1 played vital roles in autophagy process [54-56]. The induction of autophagy has been reported to be essential for survival and differentiation of monocytes [57]. Therefore, DAZAP1 and GABARAPL2 might regulate monocytes infiltration through activating autophagy process.

Interestingly, there are shared potential biological pathways between the epidemiology and risk factors in cancer progression and cardiovascular disease [58]. In addition, chemotherapeutic drugs used in cancers can cause cardiovascular diseases that affect the long-term prognosis and quality of life of patients [59]. DAZAP1 and GABARAPL2 are closely associated with several cancers [34, 36]. In our study, pan-cancer analysis revealed that DAZAP1 was a risk factor for ACC, KIRC, LGG, LIHC, MESO, and SARC, and a protective factor for BLCA, READ, STAD, and THYM. GABARAPL2 was a protective factor for ACC, KICH, KIRC, LGG, MESO, PAAD, and SKCM, and a risk factor for BRCA, ESCA, HNSC, and STAD. The results suggest that DAZAP1 and GABARAPL2 might play an important role in multiple cancers and STAAD via shared ferroptosis-associated pathways. Furthermore, we performed drug sensitivity analysis and found that some antitumor drugs might be useful for the treatment of STAAD.

This is the first comprehensive bioinformatics analysis based on WGCNA, LASSO, and SVM-REF to explore the characteristic genes and potential signaling pathways in STAAD patients, even in pan-cancer analysis. Compared with the method of gene selection using Cytohubba used in the study of Zou et al. [60], WGCNA, LASSO, and SVM-REF have a more robust power in identifying characteristic genes. However, there were several limitations to our study. First, although two datasets were merged into one dataset for analysis, the sample size was not adequately large. Second, only public datasets were utilized in our study; further *in vivo* and *in vitro* experiments are needed to validate our results.

Taken together, ferroptosis-associated DAZAP1 and GABARAPL2 might serve as potential diagnostic biomarkers for STAAD. Meanwhile, DAZAP1 and GABARAPL2 might be related to cancer and STAAD in terms of ferroptosis, which provides insights into developing new therapeutic approaches for STAAD.

Acknowledgements

We thank LetPub (www.letpub.com) for its linguistic assistance during the preparation of this manuscript.

Disclosure of conflict of interest

None.

Abbreviations

AD, aortic dissection; STAAD, Stanford type A aortic dissection; m6A, N6-methyladenosine; WGCNA, weighted gene co-expression network analysis; LASSO, least absolute shrinkage and selection operator; SVM-RFE, support vector machine-recursive feature elimination; SMC, smooth muscle cell; GO, Gene Ontology; KEGG, Kyoto Encyclopedia of Genes and Genome; GSEA, gene set enrichment analysis; FDEGs, ferroptosis-associated differentially expressed genes; AUC, area under the curve; ROC, receiver operating characteristic; OS, overall survival; PFS, progression-free survival.

Address correspondence to: Yu Wang and Zhifei Liu, Department of Anesthesiology, Shandong Provincial Hospital Affiliated to Shandong First Medical University, No. 324 Jingwu Road, Jinan 250021, Shandong, China. Tel: +86-15853159502; E-mail: wangyu198905@163.com (YW); Tel: +86-15965644128; E-mail: LZF_SD1989@163.com (ZFL)

References

[1] Smedberg C, Steuer J, Leander K and Hultgren R. Sex differences and temporal trends in aortic dissection: a population-based study of inci-

dence, treatment strategies, and outcome in Swedish patients during 15 years. Eur Heart J 2020; 41: 2430-2438.
[2] Erbel R, Aboyans V, Boileau C, Bossone E, Bartolomeo RD, Eggebrecht H, Evangelista A, Falk V, Frank H, Gaemperli O, Grabenwöger M, Haverich A, Iung B, Manolis AJ, Meijboom F, Nienaber CA, Roffi M, Rousseau H, Sechtem U, Sirnes PA, Allmen RS and Vrints CJ; ESC Committee for Practice Guidelines. 2014 ESC guidelines on the diagnosis and treatment of aortic diseases: document covering acute and chronic aortic diseases of the thoracic and abdominal aorta of the adult. The Task Force for the diagnosis and treatment of aortic diseases of the European Society of Cardiology (ESC). Eur Heart J 2014; 35: 2873-2926.
[3] Jiang DS, Yi X, Zhu XH and Wei X. Experimental in vivo and ex vivo models for the study of human aortic dissection: promises and challenges. Am J Transl Res 2016; 8: 5125-5140.
[4] Hagan PG, Nienaber CA, Isselbacher EM, Bruckman D, Karavite DJ, Russman PL, Evangelista A, Fattori R, Suzuki T, Oh JK, Moore AG, Malouf JF, Pape LA, Gaca C, Sechtem U, Lenferink S, Deutsch HJ, Diedrichs H, Marcos y Robles J, Llovet A, Gilon D, Das SK, Armstrong WF, Deeb GM and Eagle KA. The international registry of acute aortic dissection (IRAD): new insights into an old disease. JAMA 2000; 283: 897-903.
[5] Cifani N, Proietta M, Tritapepe L, Di Gioia C, Ferri L, Taurino M and Del Porto F. Stanford-A acute aortic dissection, inflammation, and metalloproteinases: a review. Ann Med 2015; 47: 441-446.
[6] Pisano C, Rita Balistreri C, Fabio Triolo O, Argano V and Ruvolo G. Acute type A aortic dissection: beyond the diameter. J Heart Valve Dis 2016; 25: 764-768.
[7] Yin F, Zhang H, Guo P, Wu Y, Zhao X, Li F, Bian C, Chen C, Han Y and Liu K. Comprehensive analysis of key m6A modification related genes and immune infiltrates in human aortic dissection. Front Cardiovasc Med 2022; 9: 831561.
[8] Pape LA, Awais M, Woznicki EM, Suzuki T, Trimarchi S, Evangelista A, Myrmel T, Larsen M, Harris KM, Greason K, Di Eusanio M, Bossone E, Montgomery DG, Eagle KA, Nienaber CA, Isselbacher EM and O'Gara P. Presentation, diagnosis, and outcomes of acute aortic dissection: 17-year trends from the international registry of acute aortic dissection. J Am Coll Cardiol 2015; 66: 350-358.
[9] Chiu P and Miller DC. Evolution of surgical therapy for Stanford acute type A aortic dissection. Ann Cardiothorac Surg 2016; 5: 275-295.
[10] Shen YH, LeMaire SA, Webb NR, Cassis LA, Daugherty A and Lu HS. Aortic aneurysms and dissections series. Arterioscler Thromb Vasc Biol 2020; 40: e37-e46.
[11] Li Z, Wang J, Yu Q, Shen R, Qin K, Zhang Y, Qiao Y and Chi Y. Identification of immune-related gene signature in Stanford type A aortic dissection. Front Genet 2022; 13: 911750.
[12] Liu F, Wei T, Liu L, Hou F, Xu C, Guo H, Zhang W, Ma M, Zhang Y, Yu Q and Wang J. Role of necroptosis and immune infiltration in human Stanford type A aortic dissection: novel insights from bioinformatics analyses. Oxid Med Cell Longev 2022; 2022: 6184802.
[13] Dixon SJ, Lemberg KM, Lamprecht MR, Skouta R, Zaitsev EM, Gleason CE, Patel DN, Bauer AJ, Cantley AM, Yang WS, Morrison B 3rd and Stockwell BR. Ferroptosis: an iron-dependent form of nonapoptotic cell death. Cell 2012; 149: 1060-1072.
[14] Sampilvanjil A, Karasawa T, Yamada N, Komada T, Higashi T, Baatarjav C, Watanabe S, Kamata R, Ohno N and Takahashi M. Cigarette smoke extract induces ferroptosis in vascular smooth muscle cells. Am J Physiol Heart Circ Physiol 2020; 318: H508-H518.
[15] Chen Y, Yi X, Huo B, He Y, Guo X, Zhang Z, Zhong X, Feng X, Fang ZM, Zhu XH, Wei X and Jiang DS. BRD4770 functions as a novel ferroptosis inhibitor to protect against aortic dissection. Pharmacol Res 2022; 177: 106122.
[16] Li N, Yi X, He Y, Huo B, Chen Y, Zhang Z, Wang Q, Li Y, Zhong X, Li R, Zhu XH, Fang Z, Wei X and Jiang DS. Targeting ferroptosis as a novel approach to alleviate aortic dissection. Int J Biol Sci 2022; 18: 4118-4134.
[17] Gao H, Sun X, Liu Y, Liang S, Zhang B, Wang L and Ren J. Analysis of hub genes and the mechanism of immune infiltration in Stanford type a aortic dissection. Front Cardiovasc Med 2021; 8: 680065.
[18] Chen F, Han J and Tang B. Patterns of immune infiltration and the key immune-related genes in acute type A aortic dissection in bioinformatics analyses. Int J Gen Med 2021; 14: 2857-2869.
[19] Chen X, Kang R, Kroemer G and Tang D. Ferroptosis in infection, inflammation, and immunity. J Exp Med 2021; 218: e20210518.
[20] Mehta RH, O'Gara PT, Bossone E, Nienaber CA, Myrmel T, Cooper JV, Smith DE, Armstrong WF, Isselbacher EM, Pape LA, Eagle KA and Gilon D; International Registry of Acute Aortic Dissection (IRAD) Investigators. Acute type A aortic dissection in the elderly: clinical characteristics, management, and outcomes in the current era. J Am Coll Cardiol 2002; 40: 685-692.
[21] Januzzi JL, Isselbacher EM, Fattori R, Cooper JV, Smith DE, Fang J, Eagle KA, Mehta RH, Nienaber CA and Pape LA; International Registry

of Aortic Dissection (IRAD). Characterizing the young patient with aortic dissection: results from the international registry of aortic dissection (IRAD). J Am Coll Cardiol 2004; 43: 665-669.
[22] Goldfinger JZ, Halperin JL, Marin ML, Stewart AS, Eagle KA and Fuster V. Thoracic aortic aneurysm and dissection. J Am Coll Cardiol 2014; 64: 1725-1739.
[23] Wang P and Lu YQ. Ferroptosis: a critical moderator in the life cycle of immune cells. Front Immunol 2022; 13: 877634.
[24] Guo J, Xu B, Han Q, Zhou H, Xia Y, Gong C, Dai X, Li Z and Wu G. Ferroptosis: a novel anti-tumor action for cisplatin. Cancer Res Treat 2018; 50: 445-460.
[25] Yamada N, Karasawa T, Wakiya T, Sadatomo A, Ito H, Kamata R, Watanabe S, Komada T, Kimura H, Sanada Y, Sakuma Y, Mizuta K, Ohno N, Sata N and Takahashi M. Iron overload as a risk factor for hepatic ischemia-reperfusion injury in liver transplantation: potential role of ferroptosis. Am J Transplant 2020; 20: 1606-1618.
[26] Wang D, Xie N, Gao W, Kang R and Tang D. The ferroptosis inducer erastin promotes proliferation and differentiation in human peripheral blood mononuclear cells. Biochem Biophys Res Commun 2018; 503: 1689-1695.
[27] Li N, Jiang W, Wang W, Xiong R, Wu X and Geng Q. Ferroptosis and its emerging roles in cardiovascular diseases. Pharmacol Res 2021; 166: 105466.
[28] Kobayashi M, Suhara T, Baba Y, Kawasaki NK, Higa JK and Matsui T. Pathological roles of iron in cardiovascular disease. Curr Drug Targets 2018; 19: 1068-1076.
[29] Katunga LA, Gudimella P, Efird JT, Abernathy S, Mattox TA, Beatty C, Darden TM, Thayne KA, Alwair H, Kypson AP, Virag JA and Anderson EJ. Obesity in a model of gpx4 haploinsufficiency uncovers a causal role for lipid-derived aldehydes in human metabolic disease and cardiomyopathy. Mol Metab 2015; 4: 493-506.
[30] Sasaki K, Ono M, Takabe K, Suzuki A and Kurihara Y. Specific intron-dependent loading of DAZAP1 onto the cox6c transcript suppresses pre-mRNA splicing efficacy and induces cell growth retardation. Gene 2018; 657: 1-8.
[31] Lin YT and Yen PH. A novel nucleocytoplasmic shuttling sequence of DAZAP1, a testis-abundant RNA-binding protein. RNA 2006; 12: 1486-1493.
[32] Smith RW, Anderson RC, Smith JW, Brook M, Richardson WA and Gray NK. DAZAP1, an RNA-binding protein required for development and spermatogenesis, can regulate mRNA translation. RNA 2011; 17: 1282-1295.
[33] Huang H, Zheng J, Shen N, Wang G, Zhou G, Fang Y, Lin J and Zhao J. Identification of pathways and genes associated with synovitis in osteoarthritis using bioinformatics analyses. Sci Rep 2018; 8: 10050.
[34] Wang Q, Guo Y, Wang W, Liu B, Yang G, Xu Z, Li J and Liu Z. RNA binding protein DAZAP1 promotes HCC progression and regulates ferroptosis by interacting with SLC7A11 mRNA. Exp Cell Res 2021; 399: 112453.
[35] Chan JCY and Gorski SM. Unlocking the gate to GABARAPL2. Biol Futur 2022; 73: 157-169.
[36] Uhlen M, Zhang C, Lee S, Sjöstedt E, Fagerberg L, Bidkhori G, Benfeitas R, Arif M, Liu Z, Edfors F, Sanli K, von Feilitzen K, Oksvold P, Lundberg E, Hober S, Nilsson P, Mattsson J, Schwenk JM, Brunnström H, Glimelius B, Sjöblom T, Edqvist PH, Djureinovic D, Micke P, Lindskog C, Mardinoglu A and Ponten F. A pathology atlas of the human cancer transcriptome. Science 2017; 357: eaan2507.
[37] Eren E, Planès R, Bagayoko S, Bordignon PJ, Chaoui K, Hessel A, Santoni K, Pinilla M, Lagrange B, Burlet-Schiltz O, Howard JC, Henry T, Yamamoto M and Meunier E. Irgm2 and Gate-16 cooperatively dampen Gram-negative bacteria-induced caspase-11 response. EMBO Rep 2020; 21: e50829.
[38] Sakaguchi N, Sasai M, Bando H, Lee Y, Pradipta A, Ma JS and Yamamoto M. Role of gate-16 and gabarap in prevention of caspase-11-dependent excess inflammation and lethal endotoxic shock. Front Immunol 2020; 11: 561948.
[39] Zhu S, Huang Y and Ye C. Identification of a ferroptosis-related prognostic signature in sepsis via bioinformatics analyses and experiment validation. Biomed Res Int 2022; 2022: 8178782.
[40] Chipman LB and Pasquinelli AE. miRNA targeting: growing beyond the seed. Trends Genet 2019; 35: 215-222.
[41] Barwari T, Joshi A and Mayr M. MicroRNAs in cardiovascular disease. J Am Coll Cardiol 2016; 68: 2577-2584.
[42] Morales M and Xue X. Targeting iron metabolism in cancer therapy. Theranostics 2021; 11: 8412-8429.
[43] Jang S, Chapa-Dubocq XR, Tyurina YY, St Croix CM, Kapralov AA, Tyurin VA, Bayır H, Kagan VE and Javadov S. Elucidating the contribution of mitochondrial glutathione to ferroptosis in cardiomyocytes. Redox Biol 2021; 45: 102021.
[44] Wang Y, Zheng L, Shang W, Yang Z, Li T, Liu F, Shao W, Lv L, Chai L, Qu L, Xu Q, Du J, Liang X, Zeng J and Jia J. Wnt/beta-catenin signaling confers ferroptosis resistance by targeting GPX4 in gastric cancer. Cell Death Differ 2022; 29: 2190-2202.
[45] Shan L, Xu X, Zhang J, Cai P, Gao H, Lu Y, Shi J, Guo Y and Su Y. Increased hemoglobin and heme in MALDI-TOF MS analysis induce ferrop-

tosis and promote degeneration of herniated human nucleus pulposus. Mol Med 2021; 27: 103.
[46] Nienaber CA, Clough RE, Sakalihasan N, Suzuki T, Gibbs R, Mussa F, Jenkins MP, Thompson MM, Evangelista A, Yeh JS, Cheshire N, Rosendahl U and Pepper J. Aortic dissection. Nat Rev Dis Primers 2016; 2: 16053.
[47] del Porto F, Proietta M, Tritapepe L, Miraldi F, Koverech A, Cardelli P, Tabacco F, de Santis V, Vecchione A, Mitterhofer AP, Nofroni I, Amodeo R, Trappolini M and Aliberti G. Inflammation and immune response in acute aortic dissection. Ann Med 2010; 42: 622-629.
[48] Tieu BC, Lee C, Sun H, Lejeune W, Recinos A 3rd, Ju X, Spratt H, Guo DC, Milewicz D, Tilton RG and Brasier AR. An adventitial IL-6/MCP1 amplification loop accelerates macrophage-mediated vascular inflammation leading to aortic dissection in mice. J Clin Invest 2009; 119: 3637-3651.
[49] Cifani N, Proietta M, Taurino M, Tritapepe L and Del Porto F. Monocyte subsets, Stanford-A acute aortic dissection, and carotid artery stenosis: new evidences. J Immunol Res 2019; 2019: 9782594.
[50] Li X, Liu D, Zhao L, Wang L, Li Y, Cho K, Tao C and Jiang B. Targeted depletion of monocyte/macrophage suppresses aortic dissection with the spatial regulation of MMP-9 in the aorta. Life Sci 2020; 254: 116927.
[51] Shen WY, Luo C, Reinaldo Hurtado P, Hurtado-Perez E, Luo RY, Hu ZL, Li H, Xu JM, Zhou XF and Dai RP. The regulatory role of ProBDNF in monocyte function: implications in Stanford type-A aortic dissection disease. FASEB J 2020; 34: 2541-2553.
[52] Del Porto F, di Gioia C, Tritapepe L, Ferri L, Leopizzi M, Nofroni I, De Santis V, Della Rocca C, Mitterhofer AP, Bruno G, Taurino M and Proietta M. The multitasking role of macrophages in Stanford type A acute aortic dissection. Cardiology 2014; 127: 123-129.
[53] Liu Y, Zou L, Tang H, Li J, Liu H, Jiang X, Jiang B, Dong Z and Fu W. Single-cell sequencing of immune cells in human aortic dissection tissue provides insights into immune cell heterogeneity. Front Cardiovasc Med 2022; 9: 791875.
[54] Xia F, Fu Y, Xie H, Chen Y, Fang D, Zhang W, Liu P and Li M. Suppression of ATG4B by copper inhibits autophagy and involves in Mallory body formation. Redox Biol 2022; 52: 102284.
[55] Zheng W, Xie W, Yin D, Luo R, Liu M and Guo F. ATG5 and ATG7 induced autophagy interplays with UPR via PERK signaling. Cell Commun Signal 2019; 17: 42.
[56] Seillier M, Peuget S, Gayet O, Gauthier C, N'Guessan P, Monte M, Carrier A, Iovanna JL and Dusetti NJ. TP53INP1, a tumor suppressor, interacts with LC3 and ATG8-family proteins through the LC3-interacting region (LIR) and promotes autophagy-dependent cell death. Cell Death Differ 2012; 19: 1525-1535.
[57] Germic N, Frangez Z, Yousefi S and Simon HU. Regulation of the innate immune system by autophagy: monocytes, macrophages, dendritic cells and antigen presentation. Cell Death Differ 2019; 26: 715-727.
[58] Vincent L, Leedy D, Masri SC and Cheng RK. Cardiovascular disease and cancer: is there increasing overlap? Curr Oncol Rep 2019; 21: 47.
[59] Nonaka M, Hosoda H and Uezono Y. Cancer treatment-related cardiovascular disease: current status and future research priorities. Biochem Pharmacol 2021; 190: 114599.
[60] Zou HX, Qiu BQ, Lai SQ, Huang H, Zhou XL, Gong CW, Wang LJ, Yuan MM, He AD and Liu JC. Role of ferroptosis-related genes in Stanford type a aortic dissection and identification of key genes: new insights from bioinformatic analysis. Bioengineered 2021; 12: 9976-9990.

Table S1. Identification of FDEGs

Gene	logFC	AveExpr	t	*P*.Value	adj.P.Val	B
HELLS	0.8359227	2.3882317	4.2032991	0.0003223	0.0495268	0.3367139
CD82	0.8311592	3.5081326	4.0440796	0.0004814	0.0495268	-0.024288
FANCD2	1.5211429	1.5744555	4.0070706	0.0005284	0.0495268	-0.108005
DAZAP1	0.5841334	3.755147	3.9957799	0.0005436	0.0495268	-0.133528
YWHAE	0.5317648	4.0273574	3.9935344	0.0005467	0.0495268	-0.138602
ZEB1	-0.717438	3.308456	-3.788143	0.0009145	0.0602939	-0.601072
GABARAPL2	-0.439363	5.2581049	-3.779734	0.0009339	0.0602939	-0.619921
SUV39H1	0.569327	3.4076179	3.7271003	0.0010648	0.0602939	-0.737731
ISCU	-0.451527	5.3855562	-3.32635	0.0028592	0.1237945	-1.621868
AURKA	1.2970392	2.7740385	3.3008098	0.0030425	0.1237945	-1.67726
SAT1	0.6746701	6.0828358	3.2657087	0.003313	0.1237945	-1.753164
NUPR1	-0.520274	4.9016981	-3.263101	0.003334	0.1237945	-1.758792
EZH2	1.1887329	2.3752931	3.2368701	0.0035526	0.1237945	-1.815325
CDC25A	1.4102887	1.1530665	3.1448243	0.0044346	0.1371875	-2.012452
METTL14	-0.424355	3.1447146	-3.134785	0.0045426	0.1371875	-2.033829
VLDLR	-0.662363	3.2775932	-3.093318	0.0050166	0.142031	-2.121858
SLC1A5	0.8520257	3.453116	3.0291441	0.0058449	0.1535532	-2.257204
KIF20A	1.8871973	2.6303238	3.0025433	0.0062254	0.1535532	-2.312976
PIR	-0.48806	4.168239	-2.984791	0.0064923	0.1535532	-2.350084
YTHDC2	-0.394997	3.1741704	-2.928752	0.0074089	0.1535532	-2.466624
AKT1S1	0.4446406	2.5436438	2.9253345	0.0074686	0.1535532	-2.473702
MEF2C	-0.573616	4.6565821	-2.911467	0.0077156	0.1535532	-2.502383
FZD7	-0.780211	3.5889364	-2.880585	0.0082941	0.1535532	-2.566038
PEX12	-0.622923	0.1671568	-2.862361	0.0086546	0.1535532	-2.603461
MIB1	-0.581861	3.433729	-2.861224	0.0086775	0.1535532	-2.605791
MAPKAP1	0.4600786	3.1131903	2.8545675	0.0088132	0.1535532	-2.619432
NRAS	0.5215214	3.2160485	2.8074997	0.0098317	0.1625362	-2.715469
SLC2A12	-0.854204	3.1356008	-2.749284	0.0112459	0.1625362	-2.833222
CDKN1A	0.8167442	5.408044	2.7303563	0.0117457	0.1625362	-2.871252
PARP1	0.6034819	5.1446969	2.7054948	0.012434	0.1625362	-2.921011
SLC2A1	-0.758322	4.2254184	-2.697138	0.0126738	0.1625362	-2.937686
ATG5	-0.379667	3.810515	-2.68492	0.0130323	0.1625362	-2.96202
SLC2A6	0.7002498	2.9642501	2.6839341	0.0130616	0.1625362	-2.963981
LCN2	0.9567785	1.7915761	2.6774836	0.0132551	0.1625362	-2.976803
PGD	0.7133895	4.2249522	2.6730037	0.013391	0.1625362	-2.985699
AEBP2	-0.588874	4.3603838	-2.672196	0.0134157	0.1625362	-2.987302
CDCA3	1.8007431	1.3592944	2.6624556	0.0137163	0.1625362	-3.006616
TMSB4Y	-1.09534	1.676318	-2.662352	0.0137195	0.1625362	-3.006822
CAPG	0.6573162	2.9703705	2.6479065	0.0141771	0.1625362	-3.035398
G6PD	0.5827004	3.9427675	2.6425024	0.014352	0.1625362	-3.046068
IL6	2.539577	3.4433129	2.6278096	0.0148377	0.163938	-3.075022
SLC39A7	0.5114347	2.5801949	2.597423	0.0158913	0.1713993	-3.134636
TFRC	0.8953884	4.5875769	2.5659518	0.0170561	0.1796839	-3.195994
PGRMC1	-0.347977	5.8177972	-2.547228	0.0177864	0.1831189	-3.232309
QSOX1	0.4029206	4.6578045	2.4916685	0.0201284	0.1948412	-3.339215
CTSB	0.4146601	5.7563045	2.4909819	0.0201591	0.1948412	-3.340528
RRM2	1.3426324	1.7653906	2.4897247	0.0202153	0.1948412	-3.342932

ATG7	0.3523107	4.0988676	2.4544718	0.0218531	0.2022545	-3.410056
AHCY	0.5432805	4.6804235	2.4539664	0.0218774	0.2022545	-3.411014
NR1D2	-0.736605	3.030286	-2.433782	0.0228706	0.2072076	-3.449198
TFR2	0.7119539	1.1974064	2.4153883	0.0238118	0.2115048	-3.483838
FURIN	0.8085024	3.0151396	2.4008654	0.02458	0.2141299	-3.51108
PPARA	-0.434426	1.9965579	-2.388512	0.0252514	0.215828	-3.534177
HIF1A	0.6472224	3.5379125	2.329698	0.0286852	0.2406373	-3.643179
SIRT1	-0.428423	4.0224109	-2.320442	0.0292631	0.2410213	-3.660185
SLC25A28	0.2875183	5.1606301	2.2811701	0.0318351	0.2518381	-3.731882
NEDD4	-0.393083	3.0990802	-2.276304	0.0321677	0.2518381	-3.740713
ALOX12B	-0.716195	0.1420565	-2.275193	0.0322442	0.2518381	-3.742729
PDK4	0.8972811	5.3263126	2.2556761	0.0336134	0.2580826	-3.778022
LPCAT3	0.4355689	3.9652514	2.2357097	0.0350688	0.2647691	-3.813933
MLLT1	0.7153367	1.7034213	2.182258	0.0392506	0.2914838	-3.909073
PEBP1	-0.232076	5.859959	-2.171606	0.040136	0.2932514	-3.927857
OTUB1	0.2756531	2.7336187	2.1308619	0.0436911	0.3137023	-3.999155
MLST8	0.2668988	3.7537418	2.1239669	0.04432	0.3137023	-4.011132
AGPS	0.3761828	3.7444888	2.0862225	0.0479087	0.3338867	-4.076246

Abbreviations: FDEGs, ferroptosis-associated differentially expressed genes; FC, fold change; AveExpr, average expression.

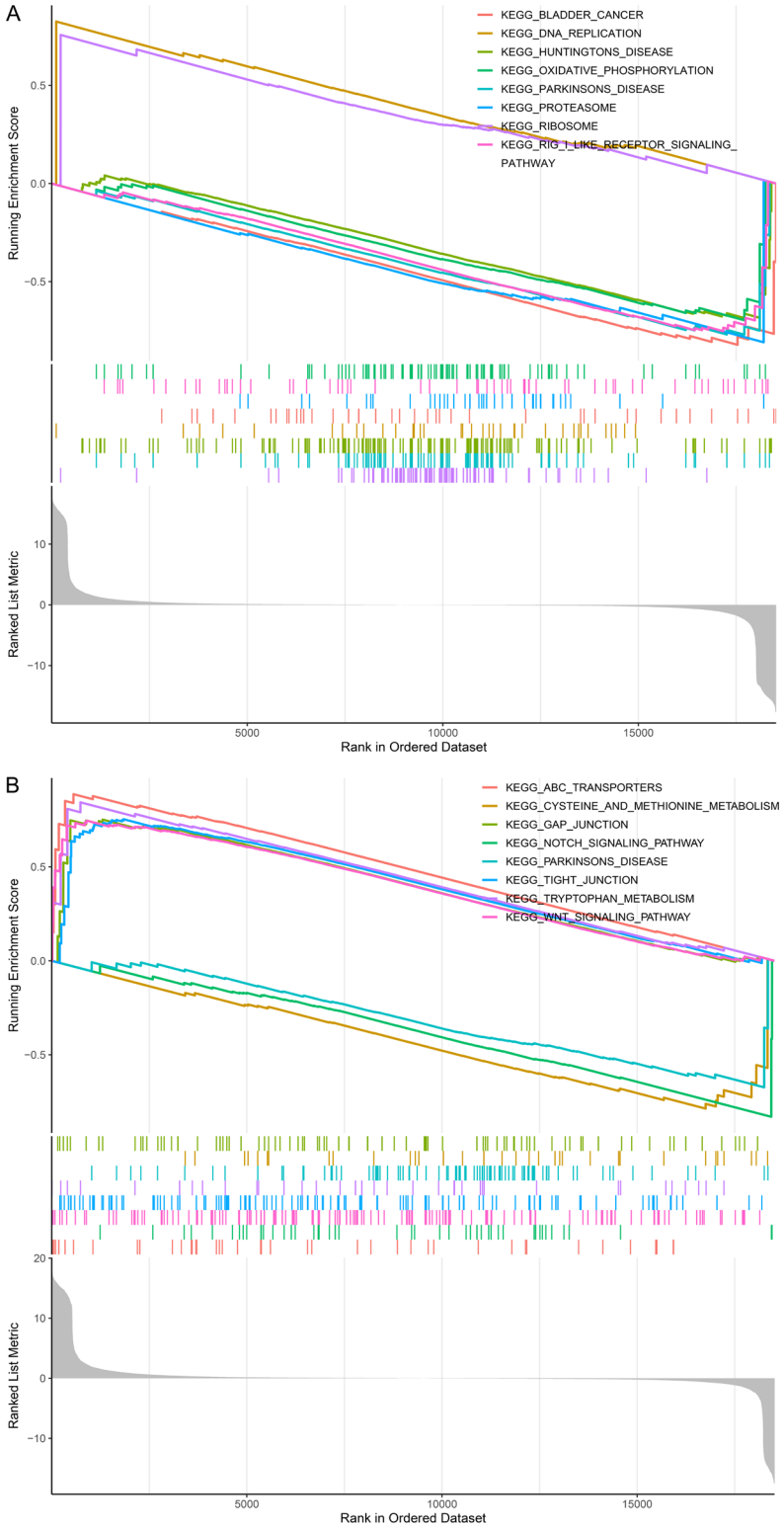

Figure S1. GSEA analysis of (A) DAZAP1 and (B) GABARAPL2. GSEA, gene set enrichment analysis.

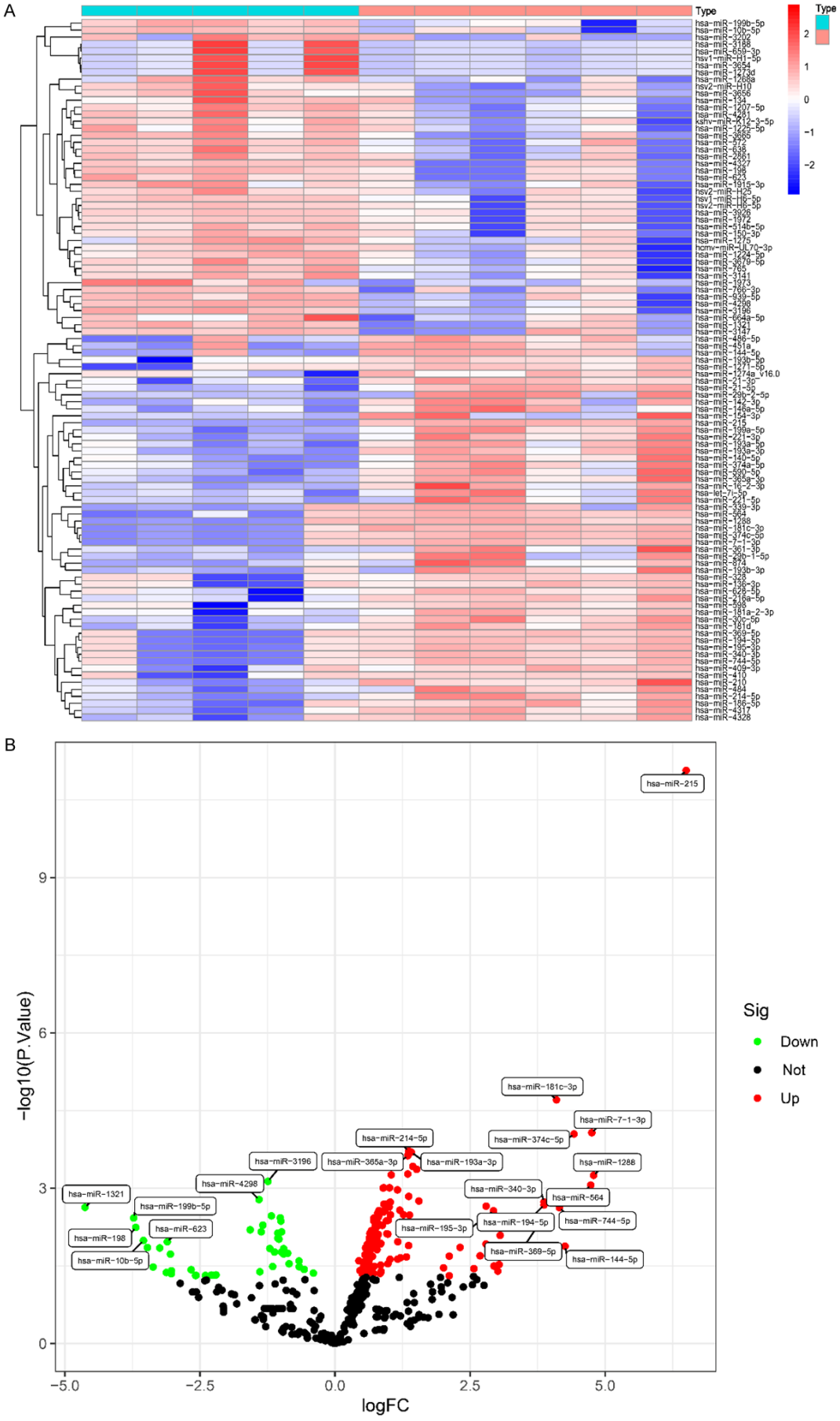
A
Type
B
hsa-miR-215
hsa-miR-181c-3p
hsa-miR-7-1-3p
hsa-miR-214-5p
hsa-miR-374c-5p
hsa-miR-3196
hsa-miR-365a-3p
hsa-miR-193a-3p
hsa-miR-1288
hsa-miR-4298
hsa-miR-340-3p
hsa-miR-1321
hsa-miR-564
hsa-miR-199b-5p
hsa-miR-195-3p
hsa-miR-194-5p
hsa-miR-744-5p
hsa-miR-623
hsa-miR-198
hsa-miR-369-5p
hsa-miR-144-5p
hsa-miR-10b-5p
−log10(P.Value)
logFC
Sig
Down
Not
Up

Figure S2. DEmiRNAs analysis. A. Heatmap of the top 50 DEmiRNAs between STAAD samples and control samples. The red represents upregulated genes, and the blue represents downregulated genes. B. Volcano plots of DEmiRNAs between STAAD samples and control samples. The red dots represent upregulated genes, the green dots represent downregulated genes and the black dots represent genes with no significant difference. DEmiRNAs, differentially expressed miRNAs; STAAD, Stanford type A aortic dissection.

Table S2. miRNAs targeted by DAZAP1 and GABARAPL2 were predicted based on StarBase database

miRNA Name	Gene Name	PITA	RNA22	miRmap	microT	miRanda	PicTar	TargetScan
hsa-miR-24-3p	DAZAP1	1	0	1	0	1	0	1
hsa-miR-199a-5p	DAZAP1	1	0	1	0	1	0	0
hsa-miR-199a-3p	DAZAP1	1	0	0	0	0	1	1
hsa-miR-7-5p	DAZAP1	1	0	0	0	1	0	0
hsa-miR-10a-5p	DAZAP1	0	0	1	1	0	0	0
hsa-miR-10a-5p	DAZAP1	1	0	1	1	1	1	1
hsa-miR-10b-5p	DAZAP1	0	0	1	1	0	0	0
hsa-miR-10b-5p	DAZAP1	1	0	1	1	1	1	1
hsa-miR-199b-5p	DAZAP1	1	0	1	0	1	0	0
hsa-miR-216a-5p	DAZAP1	1	0	1	0	1	1	0
hsa-miR-218-5p	DAZAP1	1	0	0	0	1	1	1
hsa-miR-219a-5p	DAZAP1	1	0	0	0	1	1	1
hsa-miR-9-3p	DAZAP1	0	0	1	1	0	1	0
hsa-miR-134-5p	DAZAP1	1	0	0	0	1	0	0
hsa-miR-186-5p	DAZAP1	1	0	0	0	1	0	0
hsa-miR-186-5p	DAZAP1	1	0	0	0	1	0	0
hsa-miR-320a	DAZAP1	1	0	1	1	1	1	1
hsa-miR-342-3p	DAZAP1	1	0	0	0	1	1	0
hsa-miR-339-5p	DAZAP1	0	0	1	1	1	0	0
hsa-miR-339-5p	DAZAP1	1	0	1	1	1	0	0
hsa-miR-490-3p	DAZAP1	1	0	0	0	1	0	0
hsa-miR-495-3p	DAZAP1	1	0	0	1	0	0	0
hsa-miR-508-3p	DAZAP1	1	0	0	0	0	1	0
hsa-miR-487b-3p	DAZAP1	1	0	0	0	1	0	0
hsa-miR-641	DAZAP1	1	0	1	0	0	0	0
hsa-miR-653-5p	DAZAP1	1	0	0	0	1	1	0
hsa-miR-199b-3p	DAZAP1	1	0	0	0	0	1	1
hsa-miR-455-3p	DAZAP1	1	0	1	0	0	1	0
hsa-miR-582-3p	DAZAP1	1	0	1	0	0	1	0
hsa-miR-873-5p	DAZAP1	1	0	0	0	1	0	0
hsa-miR-216b-5p	DAZAP1	1	0	0	0	1	0	0
hsa-miR-942-5p	DAZAP1	1	0	1	0	0	0	0
hsa-miR-513b-5p	DAZAP1	1	0	1	1	0	0	0
hsa-miR-513b-5p	DAZAP1	1	0	1	1	0	0	0
hsa-miR-320b	DAZAP1	1	0	1	1	1	1	1
hsa-miR-320c	DAZAP1	1	0	1	1	1	1	1
hsa-miR-1249-3p	DAZAP1	1	0	1	0	0	0	0
hsa-miR-1249-3p	DAZAP1	1	0	1	0	0	0	0
hsa-miR-320d	DAZAP1	1	0	1	1	1	1	1
hsa-miR-3129-5p	DAZAP1	0	0	0	0	0	1	1
hsa-miR-3164	DAZAP1	0	0	1	1	0	0	0
hsa-miR-4429	DAZAP1	0	0	1	1	0	1	1

hsa-miR-4731-5p	DAZAP1	0	0	1	2	0	1	0
hsa-miR-3064-5p	DAZAP1	0	0	1	1	0	1	0
hsa-miR-3064-5p	DAZAP1	0	0	1	1	0	0	0
hsa-miR-4782-3p	DAZAP1	0	0	0	0	0	1	1
hsa-miR-105-5p	GABARAPL2	1	0	1	0	0	1	0
hsa-miR-34a-5p	GABARAPL2	1	0	0	1	1	0	0
hsa-miR-204-5p	GABARAPL2	1	0	0	0	1	0	0
hsa-miR-211-5p	GABARAPL2	1	0	0	0	1	0	0
hsa-miR-200b-3p	GABARAPL2	1	0	0	1	1	0	0
hsa-miR-141-3p	GABARAPL2	1	0	0	0	1	1	0
hsa-miR-145-5p	GABARAPL2	1	0	1	1	1	1	1
hsa-miR-149-5p	GABARAPL2	1	0	0	0	1	0	0
hsa-miR-186-5p	GABARAPL2	1	0	0	0	1	0	0
hsa-miR-200c-3p	GABARAPL2	1	0	0	1	1	1	0
hsa-miR-200a-3p	GABARAPL2	1	0	0	1	1	1	0
hsa-miR-34c-5p	GABARAPL2	1	0	0	0	1	0	0
hsa-miR-374a-5p	GABARAPL2	1	0	0	0	1	0	0
hsa-miR-328-3p	GABARAPL2	0	0	1	0	1	0	0
hsa-miR-429	GABARAPL2	1	0	0	1	1	1	0
hsa-miR-449a	GABARAPL2	1	0	0	1	1	0	0
hsa-miR-494-3p	GABARAPL2	1	0	0	0	1	0	0
hsa-miR-495-3p	GABARAPL2	1	0	0	0	1	0	0
hsa-miR-509-3p	GABARAPL2	1	0	0	1	0	0	0
hsa-miR-449b-5p	GABARAPL2	1	0	0	0	1	0	0
hsa-miR-655-3p	GABARAPL2	1	0	0	0	0	1	0
hsa-miR-656-3p	GABARAPL2	1	0	0	0	0	1	0
hsa-miR-371a-5p	GABARAPL2	1	0	0	0	1	0	0
hsa-miR-501-3p	GABARAPL2	1	0	1	1	0	0	0
hsa-miR-501-3p	GABARAPL2	1	0	1	1	0	0	0
hsa-miR-502-3p	GABARAPL2	1	0	1	1	0	0	0
hsa-miR-502-3p	GABARAPL2	1	0	1	1	0	0	0
hsa-miR-455-3p	GABARAPL2	1	0	1	1	0	1	1
hsa-miR-888-5p	GABARAPL2	1	0	1	1	0	0	0
hsa-miR-541-5p	GABARAPL2	0	0	1	1	0	1	0
hsa-miR-876-5p	GABARAPL2	1	0	0	0	1	0	0
hsa-miR-374b-5p	GABARAPL2	1	0	0	0	1	0	0
hsa-miR-944	GABARAPL2	1	0	0	1	0	0	0
hsa-miR-1224-5p	GABARAPL2	1	0	1	0	0	1	0
hsa-miR-3611	GABARAPL2	0	0	1	1	0	0	0
hsa-miR-374c-5p	GABARAPL2	0	0	1	1	0	0	0
hsa-miR-374c-5p	GABARAPL2	0	0	1	1	0	1	0
hsa-miR-5195-3p	GABARAPL2	0	0	1	1	0	1	1
hsa-miR-374c-3p	GABARAPL2	0	0	1	1	0	0	0

Abbreviations: miRNAs, microRNAs.